Title
Human gut bacteria produce TH17-modulating bile acid metabolites

Journal
Nature, 603(7903)

ISSN
0028-0836

Authors
Paik, Donggi
Yao, Lina
Zhang, Yancong
et al.

Publication Date
2022-03-31

DOI
10.1038/s41586-022-04480-z

Peer reviewed

HHS Public Access

Author manuscript

Nature. Author manuscript; available in PMC 2022 September 16.

Published in final edited form as:

Nature. 2022 March ; 603(7903): 907–912. doi:10.1038/s41586-022-04480-z.

Human gut bacteria produce T_H17-modulating bile acid metabolites

Donggi Paik[1,§], **Lina Yao**[2,§], **Yancong Zhang**[3,4], **Sena Bae**[4,5], **Gabriel D. D'Agostino**[2], **Minghao Zhang**[6], **Eunha Kim**[1], **Eric A. Franzosa**[4,5], **Julian Avila-Pacheco**[3], **Jordan E. Bisanz**[7], **Christopher K. Rakowski**[8], **Hera Vlamakis**[3,11], **Ramnik J. Xavier**[3,9,10,11], **Peter J. Turnbaugh**[7,12], **Randy S. Longman**[13], **Michael R. Krout**[8], **Clary B. Clish**[3], **Fraydoon Rastinejad**[6], **Curtis Huttenhower**[3,4,5], **Jun R. Huh**[1,14,*], **A. Sloan Devlin**[2,*]

[1]Department of Immunology, Blavatnik Institute, Harvard Medical School, Boston, MA, USA.

[2]Department of Biological Chemistry and Molecular Pharmacology, Blavatnik Institute, Harvard Medical School, Boston, MA, USA.

[3]Broad Institute of MIT and Harvard, Cambridge, MA, USA.

[4]Department of Biostatistics, Harvard T. H. Chan School of Public Health, Boston, MA, USA.

[5]Department of Immunology and Infectious Diseases, Harvard T. H. Chan School of Public Health, Boston, MA, USA.

[6]Target Discovery Institute, Nuffield Department of Medicine, University of Oxford, Oxford, UK

[7]Department of Microbiology and Immunology, University of California San Francisco, San Francisco, CA, USA

[8]Department of Chemistry, Bucknell University, Lewisburg, PA, USA

[9]Center for Computational and Integrative Biology, Massachusetts General Hospital and Harvard Medical School, Boston, MA, USA

[*] jun_huh@hms.harvard.edu, sloan_devlin@hms.harvard.edu.

[§]These authors contributed equally: Donggi Paik, Lina Yao

Author contributions

J.R.H. and A.S.D. conceptualized the study. D.P., L.Y., J.R.H., and A.S.D. conceived the project and designed the experiments. D.P. performed mouse experiments, in vitro T cell and reporter assays. L.Y. performed human isolate screen, bacterial in vitro culture experiments, and BA profiling. G.D.D. performed HSDH enzyme characterization. Y.Z. and S.B. performed the bioinformatics analyses. E.A.F. and C.H. supervised the computational analyses. J.A.P. and C.C. performed LCA derivative identification in PRISM and HMP2 metabolomics. E.K. performed T cell RNA-Seq analysis. M.Z. and F.R. performed in vitro protein binding assays. J.E.B. performed comparative genomics on *E. lenta*. C.K.R. and M.R.K. synthesized some of the BA derivatives. J.E.B. and P.J.T., supervised the *E. lenta* human isolate studies. H.V. and R.J.X. provided bacterial strains and technical support. R.L. provided the patient stool samples. D.P., L.Y., Y.Z., S.B., G.D.D., E.A.F., J.R.H., and A.S.D. wrote the manuscript, with contributions from all authors.

Competing interests

A.S.D. is a consultant for Takeda Pharmaceuticals and Axial Therapeutics. J.R.H. is a consultant for CJ Research Center, LLC and Interon Laboratories and on the scientific advisory board for ChunLab. P.J.T. is on the scientific advisory board for Kaleido, Pendulum, Seres, and SNIPRbiome. C.H. is on the scientific advisory boards of Seres Therapeutics, Empress Therapeutics, and ZOE Nutrition.

Additional information

Supplementary Information is available for this paper. Correspondence and requests for materials should be addressed to Sloan Devlin (sloan_devlin@hms.harvard.edu) and Jun Huh (Jun_Huh@hms.harvard.edu). For gel source data, see Supplementary Figure 1. Reprints and permissions information is available at www.nature.com/reprints.

[10]Department of Molecular Biology, Massachusetts General Hospital and Harvard Medical School, Boston, MA, USA

[11]Center for Microbiome Informatics and Therapeutics, MIT, Cambridge, MA, USA

[12]Chan Zuckerberg Biohub, San Francisco, CA, USA.

[13]Jill Roberts Center for IBD, Weill Cornell Medicine, New York, NY, USA

[14]Evergrande Center for Immunologic Diseases, Harvard Medical School and Brigham and Women's Hospital, Boston, MA, USA.

Abstract

The microbiota modulates gut immune homeostasis. Bacteria influence the development and function of host immune cells, including T helper cells expressing interleukin-17A (T_H17 cells). We previously reported that the bile acid (BA) metabolite 3-oxolithocholic acid (3-oxoLCA) inhibits T_H17 cell differentiation[1]. While it was suggested that gut-residing bacteria produce 3-oxoLCA, the identity of such bacteria was unknown, and it was unclear whether 3-oxoLCA and other immunomodulatory BAs are associated with inflammatory pathologies in humans. Here, we identify human gut bacteria and corresponding enzymes that convert the secondary BA lithocholic acid into 3-oxoLCA as well as the abundant gut metabolite isolithocholic acid (isoLCA). Like 3-oxoLCA, isoLCA suppressed T_H17 differentiation by inhibiting RORγt (retinoic acid receptor-related orphan nuclear receptor γt), a key T_H17 cell-promoting transcription factor. Levels of both 3-oxoLCA and isoLCA and the 3α-hydroxysteroid dehydrogenase (3α-HSDH) genes required for their biosynthesis were significantly reduced in inflammatory bowel disease (IBD) patients. Moreover, levels of these BAs were inversely correlated with expression of T_H17 cell-associated genes. Overall, our data suggest that bacterially produced BAs inhibit T_H17 cell function, an activity that may be relevant to the pathophysiology of inflammatory disorders such as IBD.

Introduction

Bile acids (BAs) are steroidal natural products that are secreted into the GI tract postprandially, where they act as detergents that aid in digestion and as ligands for host receptors[2,3]. In the gut, host-derived primary BAs are metabolized by resident microbes to form a large group of compounds called secondary BAs[3]. Both primary and secondary BAs regulate host metabolism[2,4] and immune responses[5–8].

BAs modulate the differentiation and function of T cells, including inflammatory T_H17 cells and anti-inflammatory regulatory T (T_{reg}) cells, which help protect against extracellular pathogens and maintain host immune tolerance, respectively[9–13]. Specifically, secondary BAs such as isoallolithocholic acid (isoalloLCA) and isodeoxycholic acid (isoDCA)[1,15 14] modulate the differentiation of T_{reg} cells. In addition, 3-oxoLCA inhibits T_H17 cell differentiation by blocking the function of the nuclear hormone receptor (NhR) RORγt[1,16,17]. 3-oxoLCA is absent from the ceca of germ-free (GF) B6 mice[1], indicating that gut bacteria may synthesize 3-oxoLCA. However, it is unknown which commensal bacteria and bacterial enzymes produce 3-oxoLCA (Fig. 1a) and whether this compound

or additional secondary BAs that modulate T_H17 cell responses are implicated in the pathogenesis of IBD.

Here, we use a screen of human isolates to identify gut bacteria that produce 3-oxoLCA as well as an abundant gut metabolite, isolithocholic acid (isoLCA), which we demonstrate inhibits T_H17 cell differentiation. Multi-omics analyses of two IBD registries revealed that 3-oxoLCA and isoLCA as well as bacterial genes responsible for their production were negatively associated with IBD and T_H17-related host gene expression. Together, our data suggest that bacterial production of 3-oxoLCA and isoLCA may contribute to gut immune homeostasis in humans.

Results

Screen for 3-oxoLCA-producing bacteria

We screened strains isolated from human stool for their ability to convert LCA into 3-oxoLCA. LCA is present in high concentrations in human cecal contents (mean ~160 μM)[18] and we reasoned that gut bacteria might be able to oxidize the C3-hydroxyl group of LCA to produce 3-oxoLCA (Fig. 1a). After testing stool from 15 individuals, we used the two samples that contained the highest 3-oxoLCA levels in the screen (p#3 and p#27, Extended Data Fig. 1a). We established a library of 990 culturable isolates comprised of a diverse array of bacteria, with members from all of the major gut phyla represented (Extended Data Fig. 1b–d, see Methods).

A total of 238 bacterial isolates converted LCA to 3-oxoLCA after 48 hours. These producers belonged to 12 genera (Table S2). Among these, the top producers included *Gordonibacter pamelaeae* P7-E3, *Eggerthella lenta* P7-G7, *Raoultibacter massiliensis* P7-A2, *Collinsella intestinalis* P8-C1, *Adlercreutzia equolifaciens* P11-C8, and *Clostridium citroniae* P2-B6 (Fig. 1b). Consistent with our findings, an early study showed that isolates of *Eubacterium lentum* (later reclassified as *Eggerthella lenta*) could produce small amounts of 3-oxoLCA in anaerobic resting cell culture[19]. The type strains of a subset of these organisms produced a comparable amount of 3-oxoLCA in vitro (Extended Data Fig. 1e). Taken together, these data indicate that human gut bacteria from an array of families within the Actinobacteria and Firmicutes phyla produce 3-oxoLCA. Supernatant from *E. lenta* cultures incubated with LCA significantly inhibited the differentiation of naive CD4+ T cells isolated from wild-type C57BL/6J (B6Jax) into T_H17 cells (Fig. 1c, d) without altering T_{reg} differentiation (Extended Data Fig. 2a, b). These data suggest that human gut bacteria producing 3-oxoLCA can suppress T_H17 cell differentiation in vitro.

IsoLCA inhibits T_H17 cells

We observed that *G. pamelaeae*, *E. lenta*, *C. citroniae* and a *Ruminococcus gnavus* isolate (P4-G2) produced a new peak (retention time 5.7 min, Fig. 1b) in addition to 3-oxoLCA. Because this compound had an identical m/z (mass-to-charge ratio) to LCA and *E. lenta* and *R. gnavus* type strains convert DCA into isoDCA, the 3β-OH isomer of DCA[20], we reasoned that this unknown metabolite was the LCA isomer isoLCA. Spike-in of pure isoLCA into bacterial cultures confirmed that the unknown compound was isoLCA (Extended Data

Fig. 2c). After LCA (mean ~160 μM) and DCA (mean ~200 μM), isoLCA is the most abundant BA in healthy human cecal contents (mean ~50 μM)[18]. Although isoLCA is largely enterohepatically reabsorbed[18], micromolar concentrations are still found in human feces (mean 54 μM, Extended Data Fig. 1a). IsoLCA is undetectable in the cecal contents of GF B6 mice[1]. Together, these data indicate that members of the microbiome produce the abundant gut metabolite isoLCA (Table S2).

We next investigated whether isoLCA also affects T helper cell differentiation. IsoLCA inhibited the differentiation of naive CD4+ T cells into T_H17 cells as efficiently as 3-oxoLCA, while another abundant iso BA, isoDCA, did not inhibit differentiation (Fig. 2a, b). While isoLCA caused a dose-dependent reduction in T_H17 cell differentiation with no significant effect on cell viability or total cell number (Extended Data Fig. 3a–c), it had no effect on T_H1 and T_{reg} cell differentiation (Extended Data Fig. 3d–g). These data suggest that like 3-oxoLCA, isoLCA may also function as a specific inhibitor of T_H17 cell differentiation.

Consistent with our in vitro observations, isoLCA treatment (0.3% w/w in chow) of B6Jax mice gavaged with segmented filamentous bacteria (SFB)-rich fecal material[21] resulted in significant reduction in T_H17 cell differentiation without affecting the T_{reg} cell population (Fig. 2c–f and Extended Data Fig. 3h). At steady state, isoLCA treatment reduced the levels of pre-existing T_H17 cells in the ileal lamina propria of SFB-colonized C57BL/6N (B6Tac) mice compared to chow-fed mice (Extended Data Fig. 3i–k). IsoLCA treatment also significantly lowered the T_H17 cell population frequency without affecting the T_{reg} population in the ileal lamina propria of mice treated with anti-CD3 (Extended Data Fig. 3l–o)[22]. These data indicate that isoLCA treatment suppresses T_H17 cell differentiation in mice at a steady state and under inflammatory conditions.

Based on the structural similarities between isoLCA and 3-oxoLCA, which both possess C3 oxygenation oriented toward the β face of the steroidal A ring, we hypothesized that isoLCA may also target RORγt (Fig. 2g). Like 3-oxoLCA, isoLCA treatment reduced RORγt reporter activity in HEK 293 cells, suggesting that isoLCA inhibits transcriptional activity of RORγt (Extended Data Fig. 3p). IsoLCA bound directly to the RORγt ligand binding domain with equilibrium dissociation constants of 7.3 μM and 24 μM based on differential scanning fluorimetry (DSF) and surface plasmon resonance (SPR) measurements, respectively (Extended Data Fig. 3q–v). These values that are within the range of physiologically relevant concentrations of isoLCA in human cecal contents[18]. In contrast, the structurally similar compound isoDCA did not exhibit reliable binding to the RORγt protein.

We next performed RNA sequencing analyses with CD4 T cells isolated from wild-type- (WT) or RORγt-deficient- (KO) mice. We identified 291 genes that were differentially regulated by isoLCA or 3-oxoLCA treatment. Consistent with the interactions of these compounds with RORγt, a subset of isoLCA- or 3-oxoLCA- affected genes (46 genes) were also similarly regulated by RORγt (Extended Data Fig. 3w). Gene ontology enrichment analysis with these 46 genes revealed that isoLCA and 3-oxoLCA treatment altered expression of genes involved in IL-17-mediated signaling and cytokine production pathways

(Extended Data Fig. 3x). These analyses indicate that isoLCA, like 3-oxoLCA, affects the T_H17 cell program by directly binding to RORγt protein and suppressing its transcriptional activity leading to changes in multiple immune-related processes.

HSDHs produce 3-oxoLCA and isoLCA

We had previously shown that gut bacteria convert DCA into 3-oxoDCA using a 3α-hydroxysteroid dehydrogenase (3α-HSDH) and 3-oxoDCA into isoDCA using a 3β-hydroxysteroid dehydrogenase (3β-HSDH)[20]. We reasoned that an analogous biosynthetic pathway was responsible for the conversion of LCA into 3-oxoLCA and then isoLCA (Fig. 3a). We therefore incubated the 990 isolates used in the first screen with 3-oxoLCA (100 μM) as the substrate. A total of 266 isolates converted 3-oxoLCA to isoLCA, and 54 isolates demonstrated more than 50% conversion. Overall, the producers belonged to 15 bacterial genera (Table S2). Several strains, including *Lactobacillus rogosae* P2-F2, *Lachnospira pectinoschiza* P2-A2, and *Catenibacterium mitsuokai* P1-A4 exhibited more than 80% conversion of 3-oxoLCA to isoLCA (Fig. 3b). The type strains of a subset of these isolates produced a comparable amount of isoLCA in vitro (Extended Data Fig. 2d). These data also suggest that collaborative metabolism by several bacterial species could contribute to the production of isoLCA.

We next sought to identify bacterial enzymes that convert LCA into 3-oxoLCA and isoLCA. Heterologous expression of *E. lenta* and *R. gnavus* HSDH candidate genes[20] followed by incubation with LCA or 3-oxoLCA revealed that Elen_0690 and Rumgna_02133 convert LCA to 3-oxoLCA while Elen_1325 and Rumgna_00694 convert 3-oxoLCA to isoLCA (Fig. 3c–d and Extended Data Fig. 4a, b). Thus, we propose that the former genes are 3α-HSDHs and the latter are 3β-HSDHs.

While the majority of the identified isoLCA-producing bacteria are Gram-positive Firmicutes or Actinobacteria, we also found that the prevalent Gram-negative human gut commensal[23] *Bacteroides fragilis* is a robust isoLCA producer. To identify the *B. fragilis* 3β-HSDH, we heterologously expressed candidate genes identified using BLASTP searches and secondary structure homology predictions (Table S3). Incubation of cell lysates with 3-oxoLCA followed by quantification of isoLCA allowed us to identify BF3538 and BF3932 as 3β-HSDHs that produce isoLCA (Fig. 3d and Extended Data Fig. 4c). Of the two genes, only when BF3538 was deleted[24] did *B. fragilis* cultures lose the ability to convert 3-oxoLCA to isoLCA (Fig. 3e). These data indicate that BF3538 encodes a 3β-HSDH that is responsible for isoLCA production in *B. fragilis* cells.

To determine whether the two 3α-HSDHs we identified (Elen_0690 and Elen_0360) are functional in growing bacteria, we utilized a collection of *Eggerthella* and *Gordonibacter* human isolates with sequenced genomes. Through comparative genomics, we identified three *E. lenta* strains (*E. lenta* Valencia, *E. lenta* 28B, *E. lenta* DSM15644) that lack a homolog for Elen_0690 and two *Gordonibacter* strains (*G. pamelaeae* 3C and *G. species* 28C) that lack a homolog for Elen_0360 (Table S4). Neither 3-oxoLCA or isoLCA were detected when *E. lenta* Valencia, *E. lenta* DSM15644, or *E. lenta* 28B were cultured with LCA, while *G. pamelaeae* and *G.* species 28C produced similar amounts of 3-oxoLCA and isoLCA from LCA as control strains containing homologs of both genes (Fig. 3f).

These data support the hypothesis that Elen_0690 and its homologs, but not Elen_0360 and its homologs, encode 3α-HSDHs responsible for the conversion of LCA to 3-oxoLCA. Similarly, we assessed whether gene-level differences could help confirm the HSDHs in *R. gnavus*. After incubating 13 strains of *R. gnavus* with LCA for 48 hours, we determined that six *R. gnavus* strains did not convert LCA to either 3-oxoLCA or isoLCA. These results are consistent with BLASTP search results indicating that these six strains do not possess a 3α-HSDH homolog (Rumgna_02133; Table S5; Extended Data Fig. 4i, j). Together, these results reveal the biosynthetic pathway for the conversion of LCA to 3-oxoLCA and isoLCA by *E. lenta* and *R. gnavus* and for the conversion of 3-oxoLCA to isoLCA by *B. fragilis*.

T_H17 differentiation was significantly reduced in cells treated with *E. lenta* DSM2243 (3α-HSDH$^+$) + LCA supernatant compared to those treated with supernatant from either *E. lenta* DSM15644 (3α-HSDH$^-$) + LCA or *E. lenta* DSM2243 alone (Extended Data Fig. 4k, l). These data suggest that the presence of 3α-HSDH in *E. lenta* affects this organism's ability to modulate T_H17 cell differentiation. Moreover, co-incubation of *E. lenta* DSM2243 (3α-HSDH$^+$) with *B. fragilis* NCTC9343 resulted in conversion of LCA to both 3-oxoLCA and isoLCA, while no conversion was observed when *E. lenta* DSM15644 (3α-HSDH$^-$) was co-incubated with *B. fragilis* ΔBF3538 (3β-HSDH$^-$) (Extended Data Fig. 4m). These data support a model of synergy for isoLCA production between strains with 3α- and 3β-HSDH activity.

Bacteria produce 3-oxoLCA/isoLCA in vivo

We next assessed whether gut bacteria could metabolize LCA in vivo. B6 GF mice were colonized with *E. lenta* DSM2243 (3α-HSDH$^+$) or *E. lenta* DSM15644 (3α-HSDH$^-$). Because LCA is absent from GF animals, colonized mice were then fed chow alone or chow supplemented with LCA (0.3% w/w) (Fig. 4a)[25]. Significantly higher levels of 3-oxoLCA were detected in the cecal contents of 3α-HSDH$^+$-colonized mice compared to those of 3α-HSDH$^-$-colonized mice (mean 34 picomol/mg wet mass vs mean 6 picomol/mg wet mass, $p<0.0001$) (Fig. 4b).

We then asked whether collaborative metabolism by gut bacteria can enhance the production of 3-oxoLCA and isoLCA in vivo. B6 GF mice were co-colonized with *E. lenta* DSM2243 and *B. fragilis* NCTC9343 and then fed chow supplemented with LCA (0.3% w/w). Co-colonized mice harbored a higher total concentration of 3-oxoLCA and isoLCA in cecal contents than mice colonized with *E. lenta* DSM2243 or *B. fragilis* alone (Fig. 4b, c). The apparent production of 3-oxoLCA by *B. fragilis*-colonized in mice may be explained by the in vivo activation of reversible 3αHSDH genes, as putative HSDH genes from the type strain converted 3-oxoLCA to LCA in vitro (Extended Data Fig. 4c), and several *B. fragilis* isolates were found to convert LCA to 3-oxoLCA in vitro (Table S2).

Next, we asked whether human gut bacteria producing 3-oxoLCA and isoLCA can modulate T_H17 cell levels in vivo. Infection of GF mice with *Citrobacter rodentium* led to robust increases in the levels of T_H17 (IL-17A+ IFNγ−), IFNγ+ T_H17 (IL-17A+ IFNγ+) and T_H1 (IL-17A− IFNγ+) cells compared to control (Fig. 4d). Treatment of *C. rodentium*-infected GF mice with isoLCA resulted in reduced T_H17 and IFNγ+ T_H17 cell levels (Fig. 4e, Extended Data Fig. 5b, c). In contrast, treatment with LCA did not significantly affect levels

of these cells (Fig 4f, Extended Data Fig. 5d, e). IsoLCA feeding did not affect T_H1 and T_{reg} cells (Extended Data Fig. 5b, c), while LCA reduced the abundance of these cells (Extended Data Fig. 5d, e).

We then co-colonized GF mice with bacteria that produce either high or low levels of 3-oxoLCA and isoLCA in vitro prior to subjecting these animals to LCA feeding and *C. rodentium* infection (Fig. 4d). Of note, we observed substantial mouse-to-mouse variation in the levels of BAs in animals infected with *Citrobacter* (Extended Data Fig. 5f). Although the precise origin of this BA variability is currently unclear, differences in food uptake, high rates of recycling of BAs through enterohepatic recirculation, and possible altered host metabolism caused by *C. rodentium* infection are potential contributors[2,3]. Regardless, colonization of GF mice with high producers, compared to colonization with low producers, resulted in more robust production of 3-oxoLCA and isoLCA levels in ceca (Extended Data Fig. 5f).

Notably, mice with high cecal 3-oxoLCA and isoLCA levels exhibited significantly reduced T_H17 and IFNγ+ T_H17 cell frequencies compared to those with lower 3-oxoLCA and isoLCA levels (quartile 4 vs quartiles 1, 2 and 3, Fig. 4g, Extended Data Fig. 5g). Furthermore, high producers of 3-oxoLCA and isoLCA more robustly suppressed both T_H17 and IFNγ+ T_H17 cell levels compared to low producers (Extended Data Fig. 5h). T_H1 and T_{reg} cell percentages, which were significantly reduced in LCA-fed GF mice, were not reduced by these bacterial colonizations **(**Extended Data Fig. 5g, h**)**. *C. rodentium* load was not affected by 3-oxoLCA and isoLCA production and reduced T_H17 cell frequencies (Extended Data Fig. 5i). Altogether, these data suggest that human gut bacteria converting LCA to 3-oxoLCA and isoLCA negatively regulate T_H17 cell levels in mice in vivo.

3-oxoLCA/isoLCA altered in IBD

Consistent with the function of 3-oxoLCA and isoLCA in mice, levels of 3-oxoLCA and isoLCA were significantly decreased in CD patients (n=68) from the Prospective Registry in IBD Study at MGH (PRISM) IBD cohort[26] relative to non-IBD controls (n = 34, Fig. 4h, i, Table S6). Furthermore, within the Integrative Human Microbiome Project (HMP2/iHMP) IBD cohort[27], levels of 3-oxoLCA and isoLCA were significantly decreased in CD patients in a dysbiotic state (n=48) compared to their non-dysbiotic baselines (n = 169, Fig. 4j, k, Table S6, Extended Data Fig. 6, 7). These data indicate that the anti-inflammatory metabolites 3-oxoLCA and isoLCA are negatively associated with CD in humans.

We identified a subset of these T_H17/IL-17-related genes[27, 28] (n=21) that were differentially expressed (DE) in IBD patients from the HMP2 cohort (Methods and Table S7, 8). We then correlated these genes with LCA, 3-oxoLCA, and isoLCA along with two other control BAs, CDCA and DCA. Strikingly, 20 out of the 21 genes with FDR-significant correlations were upregulated in IBD and also displayed a significant negative correlation with 3-oxoLCA and/or isoLCA, but not with the three other BAs (Extended Data Fig. 8). These data imply that 3-oxoLCA/isoLCA may specifically contribute to IBD by biasing the T_H17/IL-17 signaling axis.

We further explored the associations between 3α- and 3β-HSDH-related microbial features and 3-oxoLCA/isoLCA during gut inflammation. Interestingly, both *E. lenta* and *R. gnavus* 3α-HSDH homologs were significantly depleted in CD and UC patients' dysbiotic samples relative to non-dysbiotic controls (Methods, Table S9, Extended Data Fig. 9a), and 3β-HSDH homologs were significantly depleted in UC patients' dysbiotic samples (Methods, Table S9, Extended Data Fig. 9b). When we controlled for phylum-level taxonomic changes, we still observed significantly lower levels of 3-oxoLCA and isoLCA and the 3α-HSDH gene in dysbiotic CD and UC patients (Extended Data Fig. 9c–f). Moreover, we found that most 3α-/3β-HSDH homologs were positively correlated with 3-oxoLCA/isoLCA in dysbiotic CD patients (Extended Data Fig. 10a). Additionally, 3-oxoLCA/isoLCA were significantly associated with species that exhibited both 3α-/3β-HSDH activity and differential abundance between dysbiosis states within each IBD phenotype (Extended Data Fig. 10b, Table S10, Methods). Collectively, these results suggest that the decreased abundances of 3-oxoLCA and isoLCA in dysbiotic IBD are linked to changes in the abundance of the 3α-/3β-HSDHs and the species that encode these enzymes.

Discussion

Here, we identified gut bacteria and enzymes that produce 3-oxoLCA and the abundant gut metabolite isoLCA, BAs that inhibit T_H17 cell function. Notably, the majority of the 3-oxoLCA- and isoLCA-producing strains that we found were not uncovered in bioinformatic searches, highlighting the importance of in vitro approaches for the discovery of bacteria with specific enzymatic activities. The findings that levels of 3-oxoLCA and isoLCA as well as the bacterial genes responsible for their biosynthesis are reduced in IBD patients suggest that bacterial production of these molecules may help to maintain homeostatic immune balance in the gut. In other work that supports this hypothesis, *E. lenta* and genes encoding 3α-HSDHs and 3β-HSDHs in this species were recently found to be correlated with early remission among IBD patients treated with anti-cytokine therapy[29]. Negative correlations between 3-oxoLCA and isoLCA and host genes in the T_H17/IL-17 signaling axis further imply that these metabolites modulate the immune response at least in part by regulating T_H17 function in humans. Consistent with the hypothesis that these metabolites promote human health, increased levels of 3-oxoLCA- and isoLCA-producing bacteria were found in centenarian individuals compared to elderly and young control subjects[30]. Our findings add to a growing list of gut microbe-metabolite pairs that control host immune responses by directly modulating a distinct subset of immune cells. Given the growing recognition of the importance of BA molecules in regulating host physiology and immune responses, gaining a deeper understanding of the role of host-microbiota networks in mediating BA biotransformations will offer us opportunities to devise therapeutic interventions for diseases such as IBD, metabolic diseases, and cancers of the enterohepatic system.

Methods

Mice

Conventionally reared animals were housed in an individually ventilated cage system (Tecniplast) at 20–22°C and 40%–55% humidity and under a 12-h light/12-h dark cycle

at the specific pathogen-free New Research Building facility of Harvard Medical School. 6–8 weeks old male C57BL/6J mice were purchased from Jackson Laboratory. 6–8 weeks old male SFB-containing C57BL/6N mice were purchased from Taconic Biosciences. GF C57BL/6NCrl mice were purchased from Charles River Laboratories and maintained in GF isolators at Harvard Medical School. For the BA feeding experiments, irradiated powder meal (Teklad Global 19% protein extruded diet, #2019) was evenly mixed with a measured amount of BA, provided in glass feeder jars, and replenished when necessary. Colonization of mice with SFB was performed using fresh fecal samples from 2–4-month-old *il23r−/− Rag2−/−* double-knockout mice of either sexes that are known to carry higher levels of SFB compared to conventional C57BL/6N mice. Fecal samples were homogenized in sterile 1X DPBS using a 100-μm cell strainer and a 5mL syringe plunger. Approximately a quarter of the mouse fecal pellet in 200 μL 1X DPBS was introduced into each mouse using a 20G gavage needle. Successful colonization was assessed by quantitative PCR using the following primers: SFB-F, 5'-GACGCTGAGGCATGAGAGCAT-3'; SFB-R, 5'-GACGGCACGAATTGTTATTCA-3'. For anti-CD3 experiments, B6Tac mice were fed a control powder chow or a powdered chow containing isoLCA (0.3% w/w) 4 days prior to anti-CD3 injection and given an anti-CD3 injection (10 μg/mouse). 3 days later, mice were euthanized, and ~10 cm of distal small intestines were harvested for lamina propria immune cell analysis. For gnotobiotic experiments, age- and sex-matched GF mice were orally gavaged with bacterial cultures and maintained in an Isocage system (Tecniplast). Control powder meal (Teklad Global 19% protein extruded diet, #2019) or a chow evenly mixed with 0.3% 3-oxoLCA (w/w) were autoclaved and provided to mice during the experiment. Successful colonization was assessed by quantitative PCR (see Table S1 for primer sequences and Table S11 for qPCR data). For *C. rodentium* infection experiments in GF mice, age- and sex-matched GF C57BL/6NCrl mice (4 to 6 weeks) were kept on control, isoLCA- (0.08, and 0.4 % w/w) or LCA-containing diets (0.012, 0.06 and 0.3 % w/w) 3 days before and orally infected with approximately $1X10^6$ colony-forming units of *C.rodentium* and sacrificed 5 days post-infection. For *C. rodentium* infection experiments in gnotobiotic mice, age- and sex-matched GF C57BL/6NCrl or Swiss Webster mice (4 to 6 weeks old) mice were colonized with co-cultures of *E. lenta* DSM2243 and *B. fragilis* wild type (high producer group), *E. lenta* DSM15644 and *B. fragilis* 3β-HSDH KO (low producer group) or *Clostridium citroniae* human isolate P2-B6 and *B. fragilis* 3β-HSDH KO (low producer group) strains for 4 days and put on an LCA-containing diet (0.3% w/w) for additional 3 days. Colonized mice were then orally infected with $1X10^4$ colony-forming units of *C. rodentium* and sacrificed 5 days post-infection. *C. rodentium* was prepared as previously described[31]. Mice were orally gavaged with 200 μl of PBS containing indicated colony-forming units. Mice were kept in the Isocage system (Tecniplast) during the experiment. Both male and female mice were used in GF and gnotobiotic experiments. All animal procedures were approved by the Institutional Animal Care and Use Committee at Harvard Medical School. Sample sizes were determined by magnitude and consistency of measurable differences based on similar previous studies to ensure statistical and biological significance[1,14]. Mice used in the in vivo testing of BAs were randomly assigned to experimental groups. Investigators were not blinded to the experimental groups due to different diet treatments and bacterial colonization conditions in animal experiments.

Chemical synthesis of 3-oxoLCA and isoLCA

3-oxoLCA was prepared in large scale by the oxidation of LCA according to a previously reported protocol[1]. Detailed synthesis methods and characterization data of isoLCA are included in Supplementary Information (Fig. S2–6).

Isolation of lamina propria lymphocytes

Harvested intestines were cut open and rinsed in ice-cold phosphate-buffered saline (PBS). Associated fats were carefully removed and incubated in pre-warmed 1XHBSS (without calcium and magnesium) supplemented with 1 mM dithiothreitol, 2 mM EDTA and 0.5% fetal bovine serum (FBS) at 37 °C for 20 min in a shaking incubator. Then, the tissues were briefly rinsed in warm RPMI and dissociated in digestion media (RPMI supplemented with 50 μg/mL Liberase ™, 50 μg/mL DNase I and 1% FBS) at 37 °C for 40 min in a shaking incubator. Mononuclear cells were collected at the interface of a 40%/80% Percoll gradient (GE Healthcare). Cells were then analyzed by flow cytometry. The distal 10 cm of the small intestine was considered ileum.

In vitro T cell culture

Naïve CD4+ (CD25− CD4+ CD25− CD62L+ CD44−) T cells were isolated from the spleens and the lymph nodes of 6–8 weeks old B6Jax mice by FACS sorting. 96-well T-bottom plates were pre-coated with 50 μL of hamster IgG (MP Biomedicals) at 37 °C for 1 hour. Following multiple washes with 1XDPBS, 40,000 naive CD4+ T cells were seeded in T cell media (RPMI supplemented with 10% fetal bovine serum, 25 mM glutamine, 55 μM 2-mercaptoethanol, 100 U/mL penicillin, 100 mg/mL streptomycin) and their T cell receptor downstream signaling pathways (TCR activation) were activated with soluble anti-CD3 (clone 145–2C11, 0.25 μg/mL) and anti-CD28 (clone 37.51, 1 μg/mL). For T_H1 cell differentiation, 100 U/mL of IL-2 (Peprotech) and 10 ng/mL of IL-12 (Peprotech) were added. For T_H17 cell differentiation, IL-6 (eBioscience, 20 ng/mL) and human TGF-β1 (Peprotech, 0.3 ng/mL) were added. For T_{reg} culture, 100 U/mL of IL-2 (Peprotech) and human TGF-β1 (Peprotech, 5 ng/mL) were added. Bacterial culture supernatants or small molecules including BAs and ML209, a highly specific RORγt inhibitor[32] were added 18 hours after TCR activation. Cells were harvested and assayed by flow cytometry on day 3.

Flow cytometry

Cells harvested from in vitro culture or in vivo mice experiments were stimulated with 50 ng/mL PMA (Phorbol 12-myristate 13-acetate, Sigma) and 1 μM ionomycin (Sigma) in the presence of GolgiPlug (BD) for 2 hours to determine cytokine expression. After stimulation, cells were stained with various surface marker antibodies supplemented with LIVE/DEAD Fixable dye for dead cell exclusion. After washing, cells were then fixed, permeabilized with a FoxP3/Transcription factor staining kit (eBioscience) and intracellularly stained for cytokines and/or transcription factors. The following antibodies were used at the indicated dilutions for staining; anti-IL-17A (1:200; eBio17B7; eBioscience #25–7177-82), anti-FoxP3 (1:100; FJK-16s; eBioscience #11–5773-82), anti-RORγt (1:100; B2D; eBioscience #17–6981-82) anti-IFNγ (1:200; XMG1.2; eBioscience #48–7311-82), anti-CD3ε (1:400; 145–2C11; eBioscience #48–0031-82), anti-CD25 (1:200; PC61.5;

eBioscience #25–0251-82) anti-CD62L (1:400; MEL-14; eBioscience #11–0621-85), anti-CD4 (1:400; RM4–5; eBioscience #56–0042-82), anti-CD45 (1:400; 30-F11; Biolegend #103128), anti-CD8α (1:200; 53–6.7; Biolegend #100744), anti-CD19 (1:200; 6D5; Biolegend #115540), anti-CD44 (1:400; IM7; Biolegend #103032), anti-CD4 (1:400; RM4–5; BD # 566407). Live/Dead Fixable viability dye Aqua (ThermoFisher) was used at 1:500 dilution. Flow cytometry data were acquired on an LSR II flow cytometer or Symphony flow cytometer (both BD) and data were analyzed with FlowJo software (TreeStar) following the gating strategy in Fig. S7.

Luciferase reporter assay

The transcriptional activity of the fusion protein of RORγt ligand-binding domain and GAL4-DNA-binding domain is reported by luciferase expression and reporter assays were conducted as previously described[1]. Briefly, 50,000 human embryonic kidney (HEK) 293FT (Invitrogen) cells per well were plated in 96-well plates in antibiotic-free Dulbecco's Modified Eagle Media (DMEM) containing 1% fetal calf serum (FCS). 16 hours later, cells were transfected with a DNA mixture containing 50 ng of firefly luciferase reporter plasmid (Promega pGL4.31 [luc2P/Gal4UAS/Hygro]), 5 ng of Renilla luciferase plasmid (Promega pRL-CMV), and 50 ng of Gal4-DNA binding domain-human RORγt-ligand-binding domain fusion protein plasmid per each well. Transfections were performed using GeneJuice (Millipore) according to the manufacturer's instructions. BAs or vehicle control were added 8 hours after transfection and luciferase activity was measured 18 hours later using the luciferase assay kits (Biotium).

RNA-seq analysis

Total RNA was isolated using Qiagen RNeasy Plus Mini Kit according to the manufacturer's protocol and quantified using Agilent TapeStation RNA assay on Agilent 4200 TapeStation instrument. Libraries were prepared using KAPA mRNA HyperPre kit following the manufacturer's instruction. Briefly, 50 ng of total RNA per sample was used to capture total mRNA and cDNA synthesis, adapter ligation, and amplification were conducted subsequently. Following clean-up, the resulting purified libraries were analyzed by Agilent High Sensitivity D1000 ScreenTape assay on Agilent 4200 TapeStation instrument. Then, the libraries were pooled equimolarly and run on an Illumina NextSeq 500 instrument with three runs: a Mid-Output 150-cycle kit and two High-Output 150-cycle kits (to obtain sufficient counts of paired-end 75bp reads). The pool was loaded for these runs at 2.1pM, with 5% PhiX spiked in as a sequencing control. The basecall files were demultiplexed through the Harvard BPF Genomics Core's pipeline, and the resulting FASTQ files were used in subsequent analysis. Raw sequencing reads were aligned to the Ensembl reference genome GRCm38 and gene counts were quantified using Salmon (v. 1.2.1)[33]. Rstudio (v. 4.0.2) and DESeq2 (v.1.28.1) was used for differential expression analysis[34] using the Wald test with Benjamini-Hochberg correction to determine adjusted p-value < 0.05. Pairwise comparisons between DMSO-treated WT cells and isoLCA- or 3-oxoLCA- treated WT cells or DMSO-treated RORγt KO cells identified 291 differentially expressed genes. Gene Ontology analysis was performed by PANTHER Overrepresentation Test (Released 2021–05-01)[35]. Heatmaps were produced using pheatmap (v.1.0.12).

Bacterial culturing

Culturing of human gut bacteria was performed in an anaerobic chamber (Coy Laboratory Products) with a gas mixture of 5% hydrogen and 20% carbon dioxide (balance nitrogen) unless otherwise stated.

Human stool microbial isolation and cultivation—Fecal samples were obtained from patients with ulcerative colitis who have undergone fecal microbiota transplant under an Institutional Review Board-approved protocol and informed consent was obtained at Weill Cornell Medicine IRB 1404014982. Human isolate screening was performed using a published protocol[36] with the following modifications. Two frozen fecal samples with the highest levels of 3-oxoLCA in the cohort were chosen (p#3 [fecal 3-oxoLCA 44 picomol/mg], and p#27 [fecal 3-oxoLCA at 83 picomol/mg], roughly 0.1 g/sample). The fecal were divided in half. One half was homogenized in reduced phosphate-buffered saline (PBS) (Genesee Scientific) and serially diluted and plated directly onto Cullen-Haiser Gut (CHG) agar[37], which consists of brain heart infusion media (Bacto BHI, BD) supplemented with 1% BBL vitamin K1-hemin solution (BD), 1% trace minerals solution (ATCC), 1% trace vitamins solution (ATCC), 5% FBS (Genesee), 1 g/L cellobiose (Sigma), 1 g/L maltose (Sigma) and 1 g/L fructose (Sigma), and further supplemented with 0.5% (w/v) arginine (Sigma), and cultured at 37 °C. The other half was treated with an equal volume of 70% (v/v) ethanol (Sigma) for 4 hours at room temperature under ambient aerobic conditions to kill vegetative cells, washed three times with PBS, and plated on CHG agar containing 0.1% sodium taurocholate (TCA, Sigma) anaerobically for spore germination. The picked colonies were restreaked to confirm purity and then cultured in 600 μL CHG media containing 0.5% arginine. Pure human isolates (990 in total) were archived and stored as glycerol stocks at −80 °C in eleven 96-well plates. To assess the diversity of the cultured isolates, we performed Genewiz 16S-EZ sequencing. Individual colonies were incubated in 600 μL CHG media with 0.5% arginine for 48 hours, after which 100 μL aliquots from each fresh culture from the same subject were pooled together. DNA extracts were prepared using Allprep Bacterial DNA/RNA/Protein Kit (Qiagen) following the manufacturer's instructions and further submitted to Genewiz for bacterial 16S-EZ sequencing (V3 and V4 hypervariable regions) using Illumina® MiSeq with 2×250 bp configuration and data analysis. To screen human isolates for LCA metabolism, isolates were retrieved from the stock plates and cultured in 600 μL CHG media containing 0.5% arginine for 48 hours at 37°C in 96-well plates. Each isolate as well as the negative controls were then diluted 1:10 in new media containing 100 μM LCA or 100 μM 3-oxoLCA for an additional 48 hours. 0.2 mL cultures were harvested and extracted. This experiment was conducted once per substrate for all isolates from the original eleven library plates. Following BA analysis (see below), we prioritized the positive metabolizers and performed 16S ribosomal RNA gene sequencing (universal 16S-F, 5'-GAGTTTGATCCTGGCTCAG-3′; universal 16S-R, 5′-GGCTACCTTGTTACGACTT-3′) to enable taxonomic characterization for individual isolates. Positive producer function was verified in biological triplicate using single culture conditions (see below).

Single culturing—Individual strains were plated from glycerol stocks onto CHG agar supplemented with 0.5% (w/v) arginine and grown for 3 days. Colonies were then inoculated

into 3 mL of CHG liquid media in Falcon™ Round-Bottom polystyrene tubes and grown for 48 hours at 37 °C to provide starter cultures, which were diluted 1:100 in triplicate into 5 mL fresh CHG media containing either 100 μM of the corresponding substrate (either LCA [Sigma] or 3-oxoLCA [Steraloids]). Cultures were grown for 48 hours at 37 °C. An aliquot of culture (0.5 mL) was harvested and used for BA quantification. The experiments were performed in triplicate and repeated twice unless otherwise stated.

Co-culturing—Starting from single colonies, individual bacterial strains were grown anaerobically for 48 hours in 3 mL of CHG media at 37 °C. These starter cultures were normalized to an OD_{600}=0.1 by dilution into fresh media. 10 μL of each normalized starter culture was diluted in 5 mL of CHG media containing 0.75% (w/v) arginine. LCA (100 μM final concentration) or T-LCA (100 μM final concentration, Steraloids) was then added into the media. Cultures were grown for 48 hours at 37 °C and 0.5 mL aliquots were harvested for BA analysis.

Bacterial supernatant assay for in vitro T cell culture—Seed cultures from brain heart infusion media (Bacto) supplemented with 5 mg/L hemin, 2.5 uL/L Vitamin K, 500 mg/L cysteine HCl (BHI+), and 1% arginine were diluted into OD_{600}=0.1 in ISP2 + 1% arginine minimal media, which consists of 4 g/L yeast extract (Bacto), 10 g/L malt extract (Sigma), 4 g/L dextrose (Sigma), 10g/L arginine, pH 7.2, containing 800 μM LCA and grew for 8 hours. Supernatants were harvested by centrifugation (12,000 g for 10 minutes) and subsequently passed through 0.2 μm syringe filters. 10 μL of supernatant was added to 200 μL T cell culture.

E. coli heterologous expression and lysis assays

Candidate genes were placed into pET28 expression vectors under an isopropyl β- d-1-thiogalactopyranoside (IPTG)-inducible operon for heterologous expression. Plasmids were transformed into BL21 expression cell lines containing either the pLysS (Elen and Rumgna) or Rosetta (BF) enhancement cassettes. A negative control of the empty pET28a vector was transformed into both cell lines. All cells were cultured at 37 °C until an OD_{600} between 0.6 and 1.0 was reached. Expression was induced by the addition of IPTG (500 μM final concentration). The cultures were incubated overnight at 18 °C and harvested the following day by centrifugation at 4,100 x g before pellets were stored at −80 °C. The pellets were thawed and resuspended in lysis buffer (50 mM Sodium Phosphate Buffer/ 300 mM NaCl/ 10% glycerol, pH = 8). Cells were lysed by sonication and the lysate clarified by centrifugation at 18,200 x g for 45 minutes. The lysate was then incubated with 100 μM substrate (LCA or 3-oxoLCA) for 6 hours at 37 °C. Mixtures were then frozen to quench the reaction and stored at −80 °C until extraction and analysis (described below). Soluble expression was confirmed by SDS-PAGE or immunoblot (Extended Data Fig. 4d–g and Fig. S1). Initial gel analysis was performed using SDS-PAGE immediately following lysate clarification using Coomassie blue staining to visualize protein bands. In the case of the *B. fragilis* candidates and select candidates from *E. lenta* and *R. gnavus*, an anti-His tag (Cell Signaling, 2365S) immunoblot was performed with transfer verified by subsequent Amido Black total protein staining.

Bile acid analyses

BA analyses were performed using a previously reported method[38]. Stock solutions of all BAs were prepared by dissolving compounds in molecular biology-grade DMSO (Sigma). These solutions were used to establish standard curves. Glycocholic acid (GCA) (Sigma) was used as the internal standard. HPLC-grade solvents were used for preparing and running UPLC-MS samples. All data is analyzed using Agilent ChemStation and expressed as percent conversions to the predicted product(s) (LCA, 3-oxoLCA, isoLCA) or concentration in μM. Note that the four isomers of LCA that have been reported in human feces, LCA, isoLCA, allolithocholic acid (alloLCA), and isoallolithocholic acid (isoalloLCA), were separable by UPLC-MS[1].

Sample preparation for native bacterial culture and *E. coli* cell lysis—Bacterial cultures or cell lysates were acidified to pH=1 using HCl (Sigma) and extracted twice with ethyl acetate (Sigma). The organic phase was collected and dried using a SpeedVac (Thermo Scientific) for 96-well plate cultures or a TurboVap (Biotage) for bacterial tube cultures or microcentrifuge tube lysates, respectively. Dried extracts were solubilized in 75% HPLC-grade methanol (EMD Millipore) in dH_2O and analyzed by UPLC-MS (Agilent Technologies 1290 Infinity II UPLC system coupled online to an Agilent Technologies 6120 Quadrupole LC/MS spectrometry in negative electrospray mode) using a published method[39,40] with modifications outlined as follows. Extracted BA solutions were injected onto a Phenomenex 1.7 μm, C18 100 Å, 100 × 21 mm LC column with a flow rate of 0.350 mL/min using 0.05% formic acid in water as mobile phase A and acetone as mobile phase B. The following gradient was applied: 0–1 min: 25–60% B, 1–5 min: 60–70% B, 5–6 min: 70–100% B, 6–7 min: 100% B isocratic, 7–8 min: 100–25% B, 8–10 min: 25% isocratic.

Sample preparation for mouse and human tissue BAs—BAs were extracted from mouse cecal and human fecal samples and quantified by UPLC-MS as previously reported[38]. GCA or β-muricholic acid (βMCA, Steraloids) was used as the internal standard for mouse and human samples, respectively. The limits of detection of individual BAs in tissues (in pmol/mg wet mass) are as follows: β-muricholic acid, 0.10; GCA, 0.25; T-LCA, 0.04; LCA, 0.12; 3-oxoLCA, 0.18; and isoLCA, 0.29.

Genomic and meta-omic sequence analysis

***B. fragilis* NCTC9343 3β-HSDHs—**BLASTP searches of the *B. fragilis* NCTC9343 genome were performed using the JGI Integrated Microbial Genomes and Microbiomes database (version 5.0 in March 2020)[40,41] with 3β-HSDHs Elen_1325 and Rumgna_00694 as query sequences using an E value cutoff of 1E-2. All candidate genes with E values below 1E-15 were selected for heterologous expression assays. Secondary structure prediction analysis using the JPRED4 server[42] was then performed on the remaining hits. The predicted structures of the known 3β-HSDHs Elen_1325 and Rumgna_00694 were compared with those of the remaining hits. The best match to the known 3β-HSDHs, BF3538 (CAH09226.1), was also selected for heterologous expression. The *B. fragilis* Δ3538 and *B. fragilis* Δ3932 mutant strains were constructed using a reported method with slight modifications[24]. Briefly, the 1 kb regions upstream and downstream of BF3538 or BF3932 were PCR-amplified, cloned into the pLGB30, and transformed into *E. coli* S17–1

λ pir chemical competent cells. E. coli S17 λ pir cells containing the desired plasmid were cultured and conjugated into the recipient strain (*B. fragilis* NCTC9343) and selected by tetracycline, and later counter-selected by rhamnose on BHI+ with 10% horse blood (Quad five, 210–500) plates. Knockout strain colonies were confirmed via PCR (Extended Data Fig. 4h and Fig. S1) and sequencing. Loss of function of the knockout strain was confirmed via UPLC-MS with 100 μM 3-oxoLCA as the substrate. Primers used are listed in Table S1.

Comparative genomic analysis—In *E. lenta* isolates, genetic variation between the *E. lenta* DSM2243 type strain and other human isolates was determined using comparative genomic analysis pipelines as previously reported in ElenMatchR v1.0.9003[43]. Elen_0360 (ACV54351.1), Elen_0690 (ACV54671.1), and Elen_1325 (ACV55294.1) for *Eggerthellaceae* isolates (Table S4). A phylogenetic tree was created using PhyloPhlAn[44] and visualized with Ggtree[45]. In *R. gnavus* isolates, Rumgna_02133 (3α-HSDH, A7B3K3.1) and Rumgna_00694 (3β-HSDH, A7AZH2.1) were used as query genes to perform BLASTP search (Table S5).

Analyzing the impact of BAs on CD4 T cells in gnotobiotic mice

Cecal levels of LCA, 3-oxoLCA, and isoLCA in *C. rodentium*- infected GF or gnotobiotic mice were analyzed by UPLC-MS. For isoLCA-fed GF mice, data were pooled from 2 experiments to generate bar graphs (Fig. 4e, Extended Data Fig. 5b) as well as scatter plots (Extended Data Fig.5c). For LCA-fed GF mice, data pooled from 3 experiments were sorted into the following quartile groups based on the levels of LCA in cecal contents; quartile 1 (Q1): 24.14–59.46 picomol/mg wet mass LCA, 5 mice; Q2, 65.97–332.53 picomol/mg wet mass LCA, 6 mice; Q3, 371.99–2162.68 picomol/mg wet mass LCA, 6 mice; and Q4, 2238.142–5389.45 picomol/mg wet mass LCA, 5 mice (Fig. 4f, Extended Data Fig. 5d). For LCA-fed mice colonized with 3-oxoLCA- and isoLCA-producing bacteria, data pooled from 6 experiments were sorted into the following quartile groups based on the levels of 3-oxoLCA and isoLCA in cecal contents; Q1, 0–46.58 picomol/mg wet mass 3-oxoLCA+isoLCA, 11 mice; Q2, 47.91–92.78 picomol/mg wet mass 3-oxoLCA+isoLCA, 12 mice; Q3, 101–174.7 picomol/mg wet mass 3-oxoLCA+isoLCA, 11 mice; and Q4, 177.26–591.59 picomol/mg wet mass 3-oxoLCA+isoLCA, 11 mice (Fig. 4g, Extended Data Fig. 5g). One-way ANOVA followed by Tukey's multiple comparison tests were used to compare the frequencies of CD4 T cells belonging to each quartile group. Population frequencies of indicated CD4 T cells were also plotted against the LCA metabolite levels and linear regression analyses were performed in Extended Data Fig. 5c, e, f, h.

Identification of LCA derivatives from PRISM and HMP2 cohorts

The raw LC-MS data were acquired using the same C18-negative mode LC-MS methods described in the HMP2 and PRISM studies[26,27,46]. Peaks of unknown ID were confirmed using authentic standards run alongside with the quality control reference stool pool generated in the HMP2 study. The LCA derivatives were confirmed by matching their *m/z* in negative mode and retention time, and subsequently verified using LC-MS/MS (Fig. S8). Extracted ion chromatograms (EICs) were generated using QualBrowser (Xcalibur 4.1.31.9; Thermo Fisher Scientific, Waltham, MA). The commercial standards used are: LCA (Sigma, L6250), 3-oxoLCA (Steraloids (C1750–000, isoLCA (Steraloids, C1475–000), isoalloLCA

(Steraloids, C0700–000), alloLCA (Steraloids, C0680–000), DCA (Sigma, D2510), 3-oxoDCA (Steraloids, C1725–000), and isoDCA (Steraloids, C1165–000). LCA peak in PRISM: FFA_Cluster_0731, m/z = 375.2898 at 12.42 min, and in HMP2: C18n_QI48, m/z = 375.2905 at 11.98 min; 3-oxoLCA in PRISM: FFA_Cluster_0722, m/z = 373.2744 at 12.63 min and in HMP2: C18n_QI6169, m/z = 373.2749 at 12.2–12.35 min; IsoLCA in PRISM: FFA_Cluster_0733, m/z = 375.2901 at 11.73 min and in HMP2: C18n_QI6230, m/z = 375.2906 at 11.31 min (Fig. S8, Table S12).

Statistical analysis of PRISM and HMP2 IBD multi-omic datasets

Data overview—We used two publicly available IBD metabolomics datasets for determining the differential abundance (DA) of BAs in disease/dysbiotic conditions, specifically 1) the Prospective Registry in IBD Study at MGH (PRISM)[26] and 2) the IBDMDB study within the integrative Human Microbiome Project (HMP2)[27]. Additional multi-omic profiles from the HMP2 were further used to associate metabolite abundance with microbial species, gene products, and host gene expression.

The PRISM dataset used is a cross-sectional cohort incorporating subjects diagnosed with Crohn's disease (CD; n = 68); ulcerative colitis (UC, n = 53); and non-IBD controls (n = 34). As with all metabolomics here, PRISM stool samples were subjected to metabolomic profiling using a combination of four LC-MS methods. Paired metagenomic profiles from PRISM samples were not used in this study. Differential abundance in the PRISM cohort was determined as described below based on diagnosis (i.e., comparing the CD and UC subpopulations with controls). Metabolomics profiles from the PRISM cohort were taken from the associated publication's supporting information[26].

The IBDMDB HMP2 comprises a longitudinal cohort containing 132 participants with CD (n = 67), UC (n = 38), and non-IBD controls (n = 27) who were followed for up to one year each. Taxonomic and functional profiles for HMP2 metagenomes (MGX), metabolomes (MBX), and host transcriptomes (HTX) were downloaded from http://ibdmdb.org in July 2020. These were based on 1,595 MGX samples, 546 MBX samples from 106 subjects (CD, n = 50; UC, n = 30; non-IBD, n = 26), and 254 HTX samples from 90 subjects (CD, n=43; UC, n=25; non-IBD, n = 22). MGX samples had been previously profiled for microbial taxonomic composition using MetaPhlAn v2.6.0[47] and for UniRef90[48]-level gene functional content using HUMAnN v2.11.0[49]. MGX and MBX samples were strictly matched for multi-omic association if they were derived from the same subject and sampling time point (yielding 461 samples from 106 participants: 50 with CD, 30 with UC, and 26 non-IBD controls). MGX and HTX samples were matched more leniently to compensate for the smaller total number of HTX samples. Specifically, we considered the first pair of MGX: HTX samples from each subject that were separated by no more than 2 weeks (yielding 71 samples from 71 individuals: 33 with CD, 21 with UC, and 17 non-IBD controls).

Identifying differentially abundant metabolites—We used separate statistical models and definitions of disease activity when determining metabolites' DA status in the PRISM and HMP2 cohorts owing to their cross-sectional vs. longitudinal designs. Specifically, PRISM subjects classified as having CD or UC were compared with non-IBD controls,

whereas HMP2 subjects were compared between “active” (dysbiotic) and “inactive” (non-dysbiotic) states within individual time courses as described previously[27]. Prior to statistical model fitting, gut metabolome profiles of PRISM and HMP2 subjects were 1) median-normalized to reduce technical sample-to-sample variation; 2) prevalence-filtered to remove low-confidence features (requiring > 30% non-zero values); and 3) log-transformed for variance-stabilization (replacing zero values with half the smallest non-zero measurement on a per-feature basis).

Differential abundance over disease phenotype (diagnosis) was determined within the PRISM cohort by evaluating the following linear model for each metabolite in base R version 4.0.2:

$$\text{metabolite} \sim (\text{intercept}) + \text{diagnosis} + \text{age} + \text{antibiotics} + \text{immunosuppressant} + \text{mesalamine} + \text{steroids}$$

Diagnosis was coded as a categorical variable (CD, UC, non-IBD control) with non-IBD control as the reference state. Age was coded as a continuous covariate and four medication exposures (use of antibiotics, immunosuppressants, mesalamine, and steroids) were coded as binary covariates. Individual medications within these broad classes (e.g., specific antibiotic treatments) were insufficiently numerous to merit separate coding.

DA status over disease activity (dysbiosis) was determined within the longitudinally sampled HMP2 cohort by evaluating the following linear mixed-effects model for each metabolite using R’s nlme package:

$$\text{metabolite} \sim (\text{intercept}) + \text{diagnosis} + \text{diagnosis:dysbiosis} + \text{age} + \text{antibiotics} + (1 \mid \text{subject})$$

Diagnosis was coded as described above in the context of the PRISM cohort. Dysbiosis within diagnosis (diagnosis:dysbiosis) was used to determine DA status, with per-diagnosis non-dysbiotic samples serving as the reference state. Age at study consent was included as a continuous covariate and per-sample antibiotics exposure as a binary covariate. A per-subject random effect was included to compensate for repeated sampling and to “absorb” potential confounders that were invariant over subjects (e.g., recruitment site).

Model coefficients of the diagnosis (PRISM) and diagnosis:dysbiosis (HMP2) terms were interpreted as DA effect sizes, and their associated two-tailed *p*-values were used to determine statistical significance (Wald’s test). Where applicable, simultaneously derived *p*-values were adjusted for multiple hypothesis testing using the Benjamini-Hochberg FDR method (Table S6; Fig. 4h–k).

Identifying differentially abundant microbial features and metabolite associations—3α- and 3β-HSDH homologs were identified based on mapping query sequences to known protein family clusters as defined in UniRef[50] (release 2014_07). We first identified the UniRef90 annotations (i.e., protein sequences with >90% amino acid identity and >80% coverage) of the genes identified as 3α- and/or 3β-HSDHs (Elen_0690 and Elen_1325 from *E. lenta*; Rumgna_02133 and Rumgna_00694 from *R. gnavus* ATCC29149; BF3538 from *B. fragilis* NCTC9343). We refer to these as “query

UniRef90s." To identify homologs of a given query UniRef90s, we collected all UniRef90 families belonging to the same UniRef50 family as the query (i.e., a set of proteins expected to have >50% identity and high coverage of the query) (Table S9). We then estimated the per-sample abundance of 3α-HSDH and 3β-HSDH homologs in HMP2 metagenomes by summing over the abundances of homologous UniRef90 sequences (which had been pre-computed using HUMAnN) (Table S9; Extended Data Fig. 9e, f).

We tested 3α-/3β-HSDH homologs for differential abundance over dysbiosis states following a very similar approach to the one introduced above in the context of HMP2 metabolomics. Gene abundance values were similarly zero-smoothed and log-transformed prior to linear model fitting within the MaAsLin 2 package[51]. The same random effects model formulation applied to HMP2 metabolomics was applied here within MaAsLin. We additionally applied this modeling approach to the abundances of microbial species for which corresponding strains had been found to express 3α-/3β-HSDH activity in vitro.

In order to associate microbial features (genes and species) with metabolites of interest within the HMP2 dataset, we computed Spearman correlations between the gene and metabolites' residual abundances from the previously described linear models (Table S10; Extended Data Fig. 10b). This procedure helps to identify correlation between features that cannot be explained by the confounding effects of covariates included in the models. Conversely, a metabolite and gene that both correlate strongly with dysbiosis would be expected to also correlate with one another in the raw data, but this would not be suggestive of a direct link between their changing abundances. Here, module residuals reflect variation in gene and metabolite abundance after subtracting differences due to dysbiosis (in addition to diagnosis, age, antibiotics use, and per-subject variation), and therefore any remaining correlation cannot be attributed to those variables. Two-tailed *p*-values associated with these Spearman correlation coefficients were subjected to FDR correction following the procedures introduced above for model coefficients.

Identifying differentially abundant host transcripts and metabolite associations—Using paired MBX and HTX samples from the HMP2 dataset, we identified human genes that were differentially expressed (DE'ed) with respect to diagnosis (note: because this analysis considers only one HTX sample per HMP2 subject, we focus on per-subject diagnosis as a phenotype rather than per-sample dysbiotic state) (Table S7–8; Extended Data Fig. 8). We performed initial normalization on raw sample-by-gene HTX count data using the voom method implemented in R's limma package[52,53]. We then used the normalized counts as a basis for linear modeling within MaAsLin 2 to detect differential gene expression:

$$\text{gene} \sim (\text{intercept}) + \text{diagnosis} + \text{antibiotics} + \text{age}$$

That is, the transformed abundance of each gene was modeled as a function of diagnosis, consent age, and antibiotics use as defined above for the HMP2 cohort. The coefficient of the diagnosis term and its FDR-adjusted *p*-value were used to determine the effect size and statistical significance of potential differential expression. Note that DE analysis was carried out in MaAsLin 2 rather than limma voom itself 1) for consistency with other linear

modeling analyses in this work and 2) to enable export of model residuals for multi-omic correlation analysis. From the subset of human DE'ed genes with FDR-adjusted $p < 0.25$, we selected a subset that was previously identified as T_H17-related[27,28]. We then followed the approach outlined above in the context of microbial features to associate residual expression of these human genes with residual metabolite expression using Spearman correlation.

Differential scanning fluorimetry (DSF) and surface plasmon resonance (SPR) for RORγ protein and BAs

Human RORγ LBD (ligand-binding domain) A265-P491 was cloned into pSJ2 and pNic_NT6HB vectors to provide constructs with N-terminal His-tag and AVI-tag. RORγ LBD was expressed in the *Escherichia coli* strain Rosetta 2 (DE3) with 0.1mM IPTG overnight induction. Constructs were purified sequentially by affinity chromatography on Ni Sepharose resin and size exclusion on Superdex 75 PG gel-filtration column. Purified protein constructs were concentrated and stored in a buffer with 20mM Tris pH8.0, 150 mM NaCl and 0.5mM TCEP. DSF was performed using Thermo Fisher QuantStudio™ 7 Flex Real-Time PCR System. Experiments were carried out in 384-well plates with 10 μL reaction volumes. Assay buffer was 20 mM HEPES (pH 7.5), 200 mM NaCl 0.5 mM TCEP and 1% v/v DMSO. 0.04 mg/ml (1.35 μM) RORγ protein was mixed with 14-point of serial dilutions of BAs ranging from 40 μM to 4.9 nM. The reactions were incubated at room temperature for 30 minutes before being measured. The Tm shifts were calculated with the Protein Thermal ShiftTM software from the RT-PCR instrument. The result graphs were generated by GraphPad Prism with dose-response fitting. SPR was carried out with Cytiva Biacore T200 system using SA chips that immobilizes N-terminal biotinylated RORγ protein. A flow cell left blank was used for referencing the sensorgrams. The reaction buffer was 20 mM HEPES (pH 7.5), 200 mM NaCl 0.5 mM TCEP and 1% v/v DMSO. 12-point of serial dilutions of each BAs ranging from 133 μM to 0.75 nM were injected over the chip with solvent corrections performed between each set. A flow cell left blank was used for referencing the sensorgrams. Affinity and kinetics were analysed using the instrument's programme.

Quantification of SFB and *C. rodentium* load

Fecal samples were disrupted in 500 μl of 143 mM Tris buffer (pH 8.0) containing 143 mM NaCl, 14.3 mM EDTA and 5.7% SDS. 500 μl of phenol:chloroform:isoamylalchol mix (25:24:1) was added and vigorously mixed by vortexing. 250 μl of supernatant was recovered following centrifugation and bacterial genomic DNA was precipitated with 2-propanol. Pellets were rinsed with 70 % ethanol, air-dried and resuspended in 500 μl Tris-EDTA buffer (pH 8.0). 1 μl of DNA samples were used for qPCR using the following primers for quantification of bacterial load. SFB_736F; GACGCTGAGGCATGAGAGCAT, SFB_844R; GACGGCACGGATTGTTATTCA[54], *espB*_F; ATGCCGCAGATGAGACAGTTG, *espB*_R; CGTCAGCAGCCTTTTCAGCTA[55]. Next, copy numbers of SFB 16s rRNA and *C. rodentium espB* genes were calculated using a standard-curve method and normalized by fecal mass.

Reporting Summary

Further information on research design is available in the Nature Research Reporting Summary linked to this paper.

Data availability

The 16S amplicon and RNA-Seq datasets are available through NCBI under BioProject ID PRJNA675599 and GEO accession number GSE179740, respectively. All MSMS acquired for standards in this study were deposited in MoNA (https://mona.fiehnlab.ucdavis.edu/) under IDs MoNA031840 to MoNA031854 (Table S12) and the ibdmdb.org data set and the metabolomics workbench study ST000923.

Code availability

The software packages used in this study are free and open source. Source code for ElenMatchR is available at github.com/turnbaughlab/ElenMatchR. MaAsLin2 is available via http://huttenhower.sph.harvard.edu/maaslin as source code and installable packages. The R package limma is available from https://www.bioconductor.org/packages/release/bioc/html/limma.html. Analysis scripts employing these packages are available from the authors upon request.

Extended Data

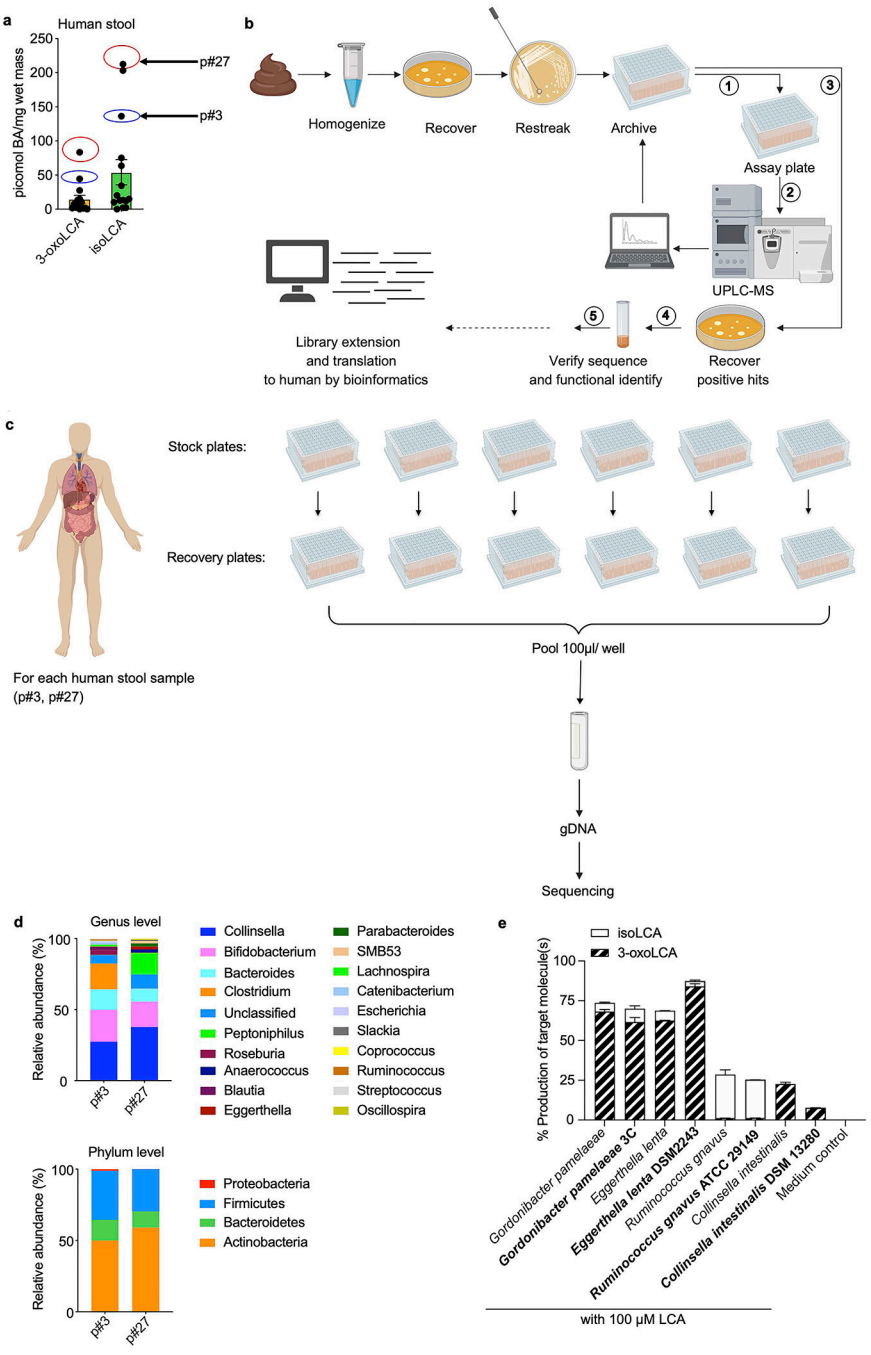

Extended Data Fig. 1 |. 3-oxoLCA biosynthetic pathway and microbial diversity from the human screen.

a, Quantification of 3-oxoLCA and isoLCA in stool samples from patients after fecal microbiota transplant (FMT) (n = 15). Stool samples from patient p#3 (3-oxoLCA: 44 picomol/mg, isoLCA: 136 picomol/mg) and patient p#27 (3-oxoLCA: 83 picomol/mg, isoLCA: 213 picomol/mg) were used to screen for 3-oxoLCA producers.

b, Schematic of the screen for bacterial producers of the LCA metabolite 3-oxoLCA from human stool samples. In total, 990 bacterial colonies were isolated, restreaked, and archived from two human stool samples. ① Replicate plates (assay plates) were then used for the screen. ② Individual isolates were incubated anaerobically with LCA (100 μM) (see Fig. 1b) or 3-oxoLCA (100 μM) (see Fig. 2b) for 48 hours. Cultures were harvested, acidified, extracted, and BA metabolites were quantified by UPLC-MS. ③ Positive hits containing 3-oxoLCA were re-selected from the archived stock plates, and recovered on new plates. ④ Activity was verified and each producer species was identified by full-length 16S rRNA sequencing. Finally, bacterial enzymes responsible for the LCA metabolite production were identified (see Fig. 3), and ⑤ corresponding genes were utilized as query sequences in BLASTP searches for novel putative bacterial producers and enzymes.

c, Sample preparation workflow for the determination of cultured bacteria from the human stool sample screen. For each patient, individual isolates were recovered and cultured for 48 hours. These isolates were then pooled together, and genomic DNA was extracted from the pooled pellet. Illumina® MiSeq sequencing on the V3 and V4 hypervariable regions of 16S rRNA was then performed.

d, Genus and phylum-level microbial community composition for each human stool sample.

e, 3-oxoLCA and/or isoLCA production was verified in the type strains of a subset of 3-oxoLCA-producing human isolates (n = 3 biological replicates per group, data are mean ± SEM).

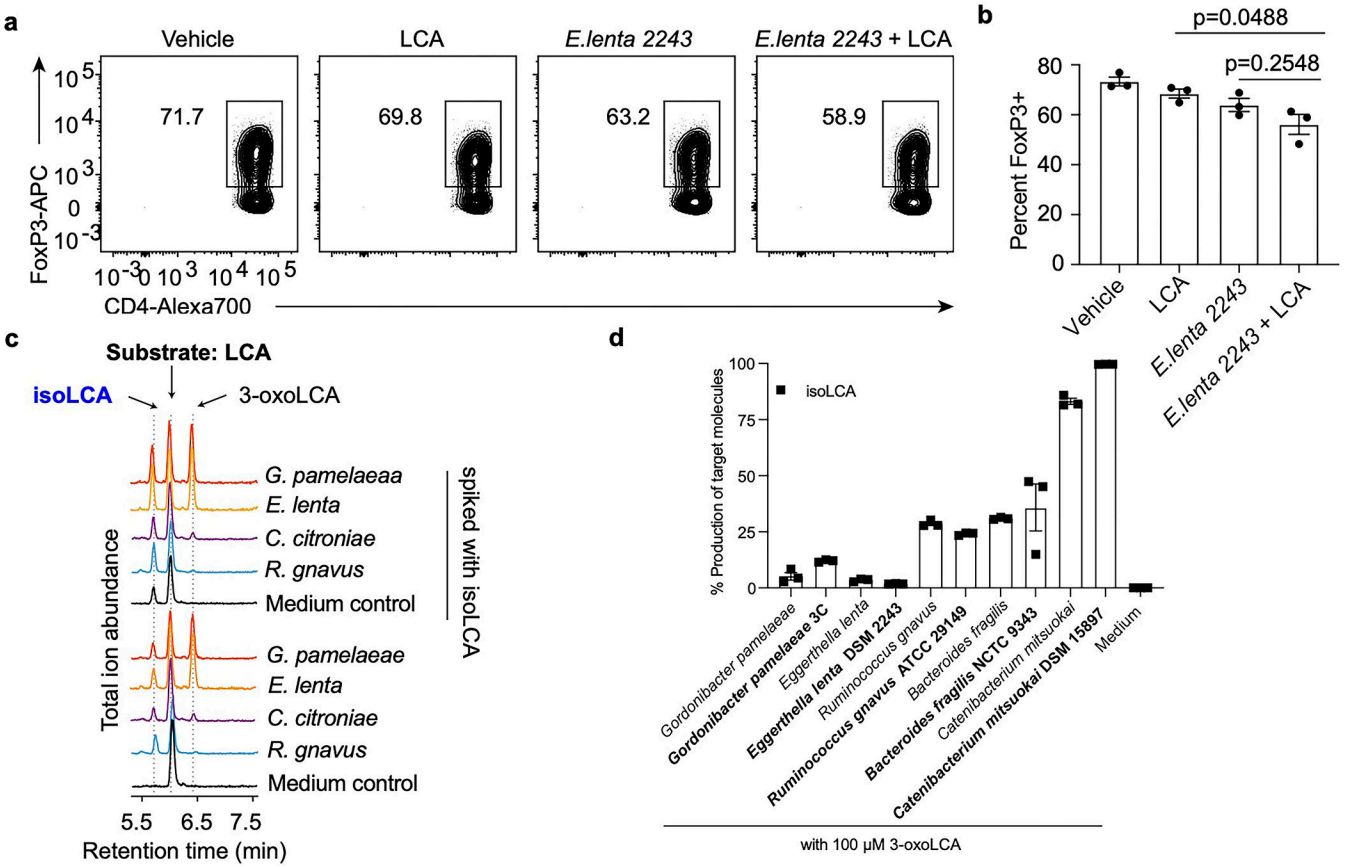

Extended Data Fig. 2 |. Supernatants from LCA metabolite-producing bacteria do not affect T_{reg} cell differentiation in vitro.

a, b, Representative FACS plots (**a**) and population frequencies (**b**) of CD4+ T cells, cultured under T_{reg} polarization conditions in vitro are presented. Bacterial culture supernatants were added 18 hours after TCR activation (n = 3 biologically independent samples per group. Data are mean ± SEM, one-way ANOVA followed by Tukey's multiple comparison test).

c, A pure standard of isoLCA was spiked into a subset of bacterial culture extracts containing the new peak (#). Co-elution and an identical m/z match confirmed that the new compound (#) in Fig. 1b was isoLCA. Total ion chromatograms (TICs) are shown.

d, isoLCA production from 3-oxoLCA (100 μM) was verified in the type strains of a subset of isoLCA-producing human isolates (n = 3 biological replicates per group, data are mean ± SEM).

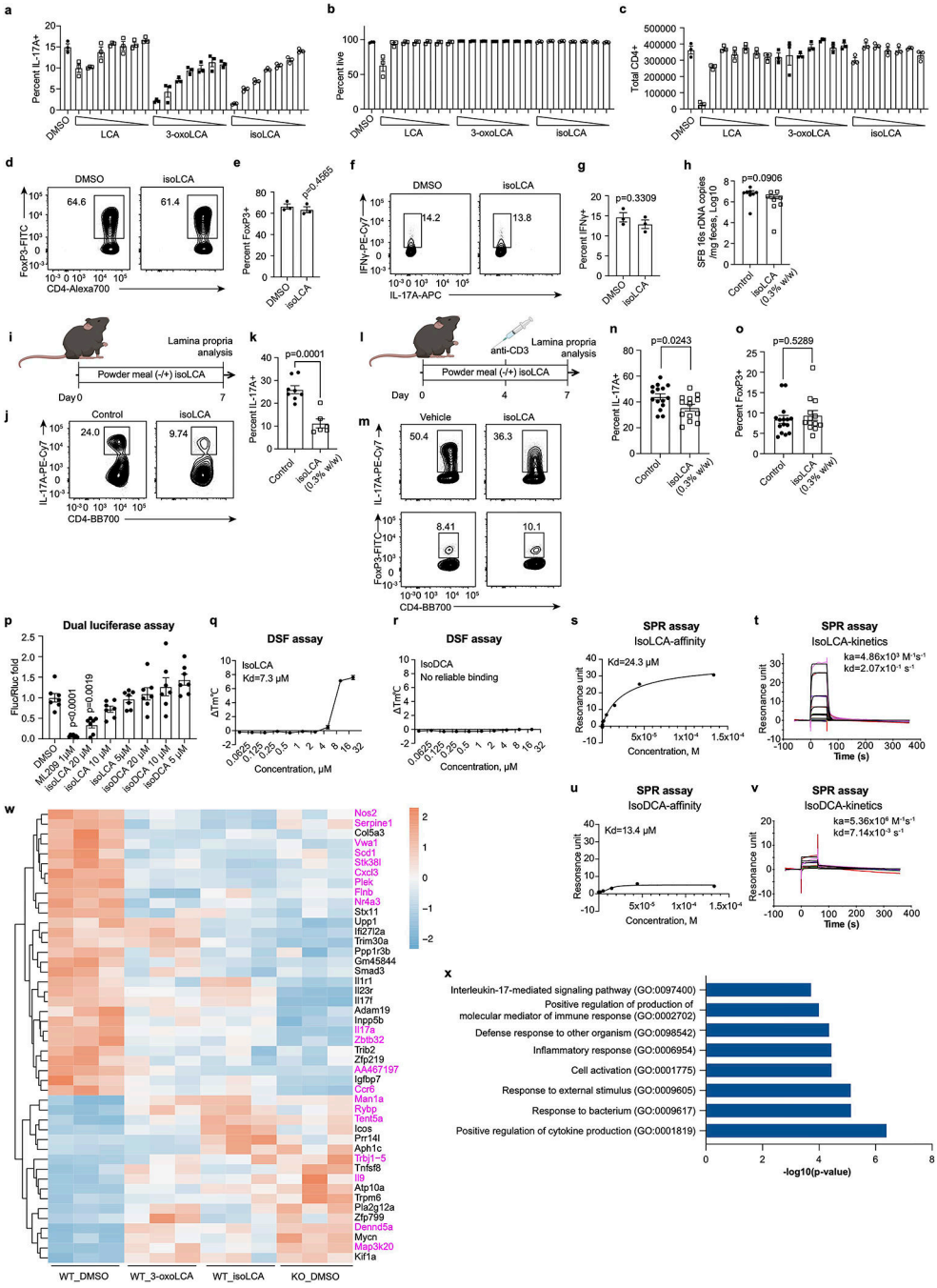

Extended Data Fig. 3 |. IsoLCA neither affects T cell viability nor inhibits T_{reg} and T_H1 cell differentiation in vitro.

a-c, IsoLCA does not reduce T cell viability or proliferation. Percentages of T_H17 cells (**a**), viable cells (**b**) and total cell numbers (**c**) at the end of T cell culture under T_H17 polarization conditions in the presence of LCA, 3-oxoLCA, or isoLCA at 40, 20, 10, 5, 2.5, 1.25 and 0.625 μM (n = 3 biologically independent samples, data are mean ± SEM, one-way ANOVA with Dunnett's multiple comparisons).

d-g, IsoLCA does not affect T_{reg} or T_H1 cell differentiation in vitro. Flow cytometry and quantification of intracellular staining for FoxP3 (**d, e**) or IFN-γ (**f, g**). Mouse naive CD4 T cells from wild-type B6Jax mice were cultured under T_H1- or T_{reg}- polarizing conditions and DMSO or isoLCA was added 18 hours after TCR activation (n = 3 biologically independent samples per condition, data are mean ± SEM, two-tailed unpaired t-test).

h, SFB colonization measured by qPCR analysis in Fig.2 c–f, calculated as SFB 16s rRNA copy number (n = 8 mice per group, pooled from two experiments, data are mean ± SEM, two-tailed unpaired t-test).

i–k, Experimental scheme of Th17 induction by SFB (**i**), representative FACS plots (**j**) and population frequencies of T_H17 cells (**k**), isolated from the ileal lamina propria of control or isoLCA-treated mice (n = 8 mice for control, n=6 mice for isoLCA-treated groups, pooled from two experiments). B6 Tac mice were fed a control or a isoLCA (0.3% w/w)-containing diet for 7 days (data are mean ± SEM, two-tailed unpaired t-test).

l–o, Experimental scheme of anti-CD3 experiment (**l**), representative FACS plots (**m**) and population frequencies of T_H17 (**n**) and T_{reg} cells (**o**) of the ileal lamina propria of control or isoLCA-treated mice (n = 15 mice for control, 13 mice for isoLCA-treated groups, pooled from three experiments). B6 Tac mice were intraperitoneally injected with anti-CD3 and fed a control diet or isoLCA-containing (0.3% w/w) diet during the experiments (data are mean ± SEM, two-tailed unpaired t-test).

p, RORγt luciferase reporter assay in HEK293 cells, treated with a synthetic RORγ inhibitor ML209 (1 μM), isoLCA (20 μM, 10 μM, 5 μM), isoDCA (20 μM, 10 μM, 5 μM) or DMSO. The fold ratio of firefly luciferase (FLuc) to Renilla luciferase (RLuc) activity is presented on the y-axis. DMSO-treated group set to 1 (n = 7 independent transfections per group, pooled from two experiments. Data are mean ± SEM, one-way ANOVA with Dunnett's multiple comparison test, vehicle set as control).

q, **r**, Differential scanning fluorimetry (DSF) analyses indicated robust binding of isoLCA (**q**), but not of isoDCA (**s**) to the RORγt ligand-binding domain (LBD).

s-v, Surface plasmon resonance (SPR) indicated robust binding of isoLCA to the RORγt LBD. Sensorgrams for affinity (**s**) and kinetics (**t**) of isoLCA and affinity (**u**) and kinetics (**v**) of isoDCA with the RORγt LBD.

w, Transcriptional profiling of wild-type (WT) T cells and RORγ deficient (KO) T cells, cultured under T_H17 cell polarization conditions. DMSO or BAs were added to cells 18 hours after TCR activation. Cells were then harvested, and RNA-sequencing was performed. Heat map represents 46 genes that are regulated by either 3-oxoLCA or isoLCA as well as RORγ (n = 3 mice per condition, the Wald test with Benjamini-Hochberg correction was used to determine FDR-adjusted p value <0.05, genes that were differentially expressed by both isoLCA and 3-oxoLCA are shown in magenta).

x, Gene ontology enrichment analysis was performed on the 46 genes that were differentially regulated by either 3-oxoLCA or isoLCA and RORγt ND revealed that these BA treatments resulted in changes in the expression of genes involved in several biological processes, including IL-17-mediated signaling and cytokine production pathways.

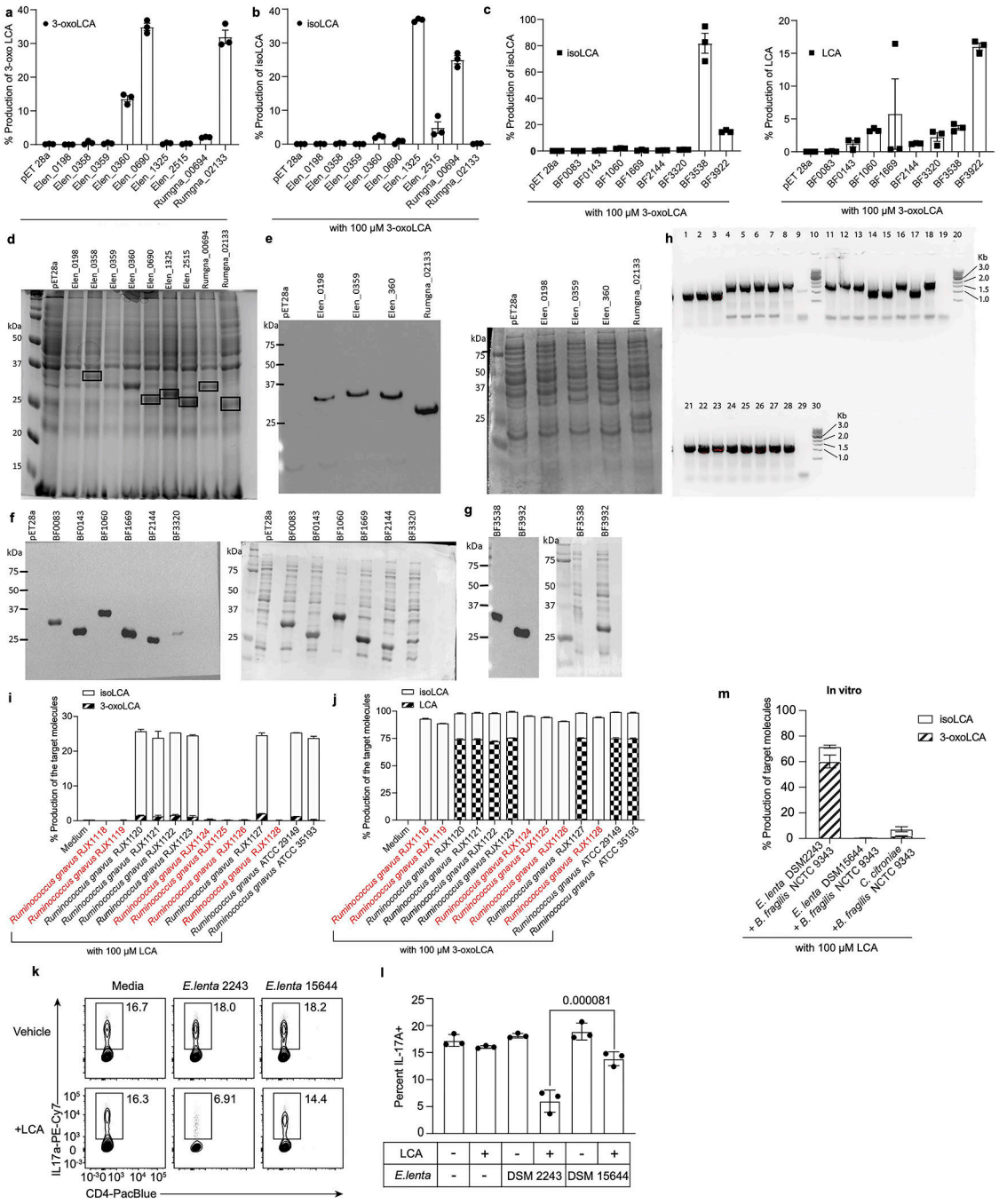

Extended Data Fig. 4 |. Screen of the candidate HSDH enzymes from gut bacteria.

a-c, Results of lysis assay in which the *E. lenta* DSM2243 (Elen), *R. gnavus* ATCC29149 (Rumgna), and *B. fragilis* NCTC9343 (BF) candidate HSDH enzymes were expressed in *E. coli* BL21 pLysS and their ability to convert LCA to 3-oxoLCA (**a**, 3α-HSDH activity), 3-oxoLCA to isoLCA (**b,** and **c**, left, 3β-HSDH activity), and 3-oxoLCA back to LCA (**d**, right, reverse 3α-HSDH activity) was analyzed by UPLC-MS. Data are reported as percent conversion to product (n = 3 biological replicates per group, data are mean ± SEM).

d-g, SDS-PAGE analysis of candidate gene expression from E. lenta DSM 2243 and R. gnavus ATCC 29149 (Elen_0358, Elen_690, Elen_1325, Elen_2515, Rumgna_00694, and Rumgna_02133) (n = 3 replicates) (**d**). Western blot of the expression of Elen_0198, Elen_0359, Elen_0360, and Rumgna_02133. Anti-His tag labeling (left). Amido black total protein stain of membrane (right) (n = 2 replicates) (**e**). Western blot of the expression of BF0083, BF0143, BF1060, BF1669, BF2144, and BF3320. Anti-His tag labeling (left). Amido black total protein stain of membrane (right) (n = 2 replicates) (**f**). Western blot of the expression of Bf3538 and Bf3932. Anti-His tag labeling (left). Amido black total protein stain of membrane (right) (n = 2 replicates) (**g**). For source gel data for **d-g**, see Fig. S1.

h, DNA gel for the *B. fragilis* genetic knockout mutants' diagnostic PCR. IntF-UHF-BF3538/ Int-R-DHF-BF3538 PCR primers: lane 1–3 are *B. fragilis* Δ3538 mutant colonies #1-#3; lane 4, 5, 7 are *B. fragilis* Δ3932 mutant colonies #1-#3; lanes 6 and 8 are *B. fragilis* WT; lane 9 is a non-template control. IntF-UHF-BF3932/ Int-R-DHF-BF3932 PCR primers: lane 11–13 are *B. fragilis* Δ3538 mutant colonies #1-#3; lane 14, 15, 17 are *B. fragilis* Δ3932 mutant colonies #1-#3; lanes 16 and 18 are *B. fragilis* WT; lane 19 is a non-template control. UNIV-16s-F/ UNIV-16s-R PCR primers: lane 21–23 are *B. fragilis* Δ3538 mutant colonies #1-#3; lane 24, 25, 27 are *B. fragilis* Δ3932 mutant colonies #1-#3; lanes 26 and 28 are *B. fragilis* WT; lane 29 is a non-template control. Lane 10, 20, 30 are the 1kb DNA ladder (n = 2 replicates). For source gel data, see Fig. S1.

i, **j,** *R. gnavus* isolates in red (*R. gnavus* RJX1118, *R. gnavus* RJX1119, *R. gnavus* RJX1124, *R. gnavus* RJX1125, *R. gnavus* RJX1126, *R. gnavus* RJX1128) that lack a homolog of Rumgna_02133 (Table S5) did not synthesize 3-oxoLCA or isoLCA from LCA (**i**). *R. gnavus* isolates in red that lack a homolog of Rumgna_02133 (Table S5) only produced isoLCA from 3-oxoLCA (**j**). All strains were incubated with 100 μM LCA as a substrate for 48 hours (n = 3 biological replicates per group).

k, **l,** The 3α-HSDH gene of *E. lenta* is required to suppress T_H17 cell differentiation in vitro. Representative FACS plots (**l**) and population frequencies of T_H17 cells (**k**) are presented. Naive CD4+ T cells from wild-type B6Jax mice were cultured under T_H17 cell polarizing conditions for 3 days. Culture supernatants of *E. lenta* DSM2243 or *E. lenta* DSM15644, an isolate lacking a 3α-HSDH, were added 18 hours after TCR activation (n=3 biologically independent samples per group, data are mean ± SEM, one-way ANOVA followed by Tukey's multiple comparison test. p=0.000081 between column 4 and 6(**l**)).

m, Production of 3-oxoLCA and isoLCA by "high" and "low" producer co-cultures. Production of 3-oxoLCA and isoLCA from LCA (100 μM) by co-cultures of human gut bacteria type strains in vitro are shown (high producer group: *E. lenta* DSM2243 + *B. fragilis* NCTC9343; low producer group: *E. lenta* DSM15644 + *B. fragilis* NCTC9343 ΔBF3538 and *C. citroniae* human isolate P2-B6 + *B. fragilis* NCTC9343 ΔBF3538; n = 3 biological replicates per co-culture, data are mean ± SEM).

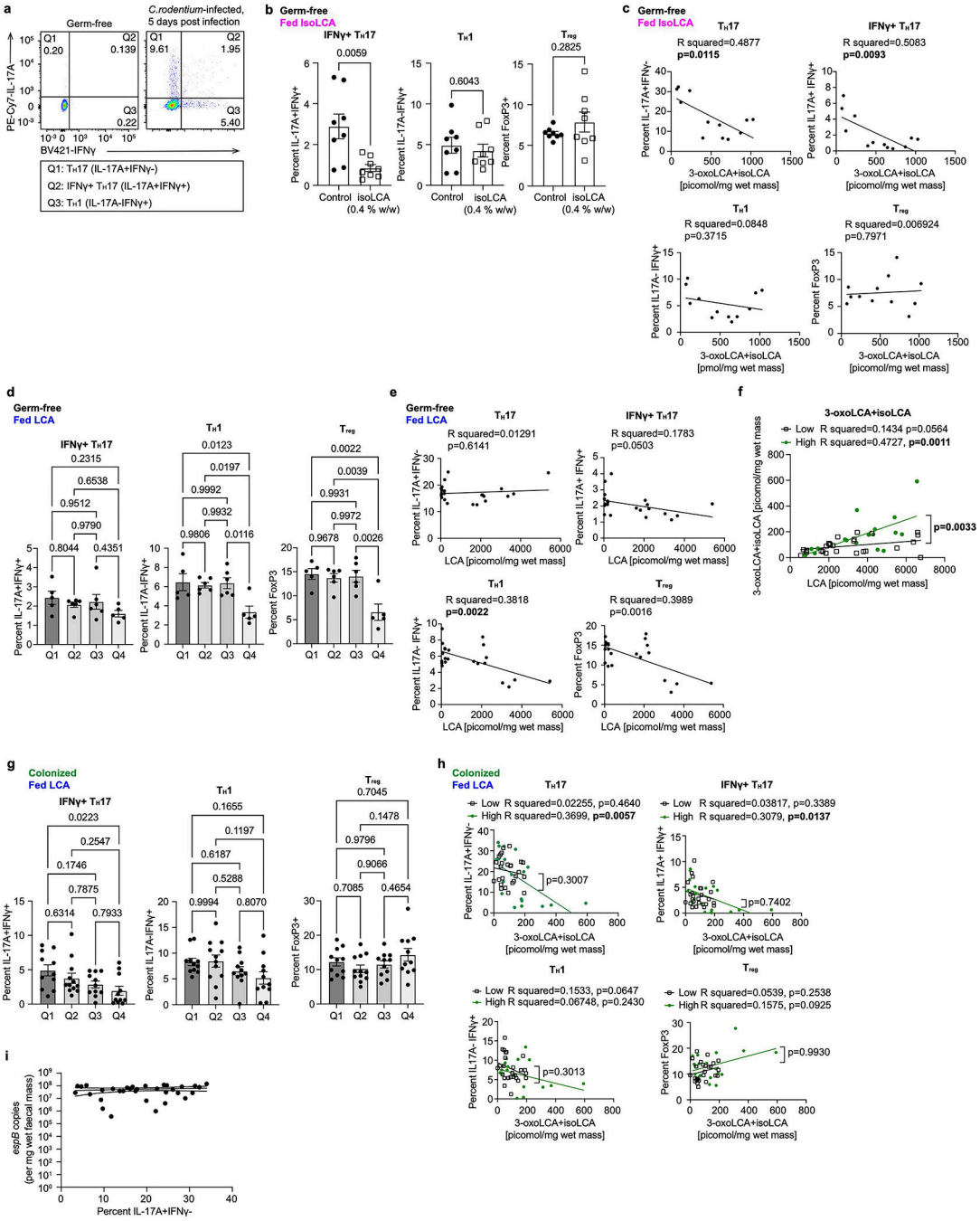

Extended Data Fig. 5 |. Human gut bacteria affect T cell levels in gnotobiotic mice.

a, Representative FACS plots for IL-17A or IFNγ- producing CD4 T cells in the colonic lamina propria of GF mice (left) or in *C.rodentium* infected mice 5 days after infection (right).

b, IsoLCA reduced IFNγ+ T_H17 cell level but did not affect T_H1 and T_{reg} cell levels in GF mice following *C. rodentium* infection (n=8 for control and isoLCA groups, data are mean ± SEM pooled from two experiments followed by two-tailed unpaired t test).

c, IsoLCA inhibited T_H17 and IFNγ+ T_H17 cell levels in a dose-dependent manner but not T_H1 and T_{reg} cell levels in GF mice treated with 0.08% or 0.4% (w/w) isoLCA-containing diet (linear regression, n=12 mice pooled from two experiments; T_H17, R-squared=0.4877, p=0.0115; IFNγ+ T_H17, R-squared=0.5083, p=0.0093; T_H1, R-squared=0.0848, p=0.3715; T_{reg}, R-squared=0.006924, p=0.7971).

d, LCA did not affect IFNγ+ T_H17 level while T_H1 and T_{reg} cell levels were negatively impacted in GF mice following *C. rodentium* infection. Mice were sorted into quartile groups based on LCA levels in cecal contents (see Methods for details, n=5 mice for Q1, n=6 for Q2, n=6 for Q3 and n=5 for Q4, data are mean ± SEM pooled from three experiments, one-way ANOVA followed by Tukey's multiple comparison test).

e, LCA treatment did not affect T_H17 and IFNγ+ T_H17 cell levels but negatively impacted T_H1 and T_{reg} cell levels in GF mice treated with 0.012%, 0.06%, 0.25% or 0.3% (w/w) LCA-containing diets (linear regression, n=22 mice; T_H17, R-squared=0.01291, p=0.6141; IFNγ+ T_H17, R-squared=0.1783, p=0.0503; T_H1, R-squared=0.3818, p=0.0022; T_{reg}, R-squared=0.3989, p=0016)

f, 3-oxoLCA and isoLCA levels in mice colonized with the high producer bacterial group were significantly higher than those colonized with the low producer groups (linear regression, R-squared=0.1434, p=0.0564, n=26 mice for low producers; R-squared=0.4727, p=0.0011, n=19 for high producers; p=0.0033 for the difference between two lines).

g, GF mice colonized with bacterial producers of 3-oxoLCA and isoLCA affected IFNγ+ T_H17 but not T_H1 or T_{reg} cell levels. Mice were sorted into quartile groups based on 3-oxoLCA+isoLCA levels in cecal contents (see Methods for details, n=11 mice for Q1, n=12 for Q2, n=11 for Q3 and n=11 for Q4, data are mean ± SEM pooled from six experiments, one-way ANOVA followed by Tukey's multiple comparison test).

h, GF mice colonized with low and high bacterial producers of 3-oxoLCA and isoLCA affected T_H17 and IFNγ+ T_H17 but not T_H1 or T_{reg} cell levels (linear regression, n=26 for low producers, n=19 mice for high producers; T_H17, R-squared=0.02255, p=0.4640 for low producers, R-squared=0.3699, p=0.0057 for high producers, p=0.3007 for the interaction term (slope*bacterial groups); IFNγ+ T_H17, R-squared=0.03817, p=0.3389 for low producers, R-squared=0.3079, p=0.0137 for high producers, p=0.7402 for the interaction term (slope*bacterial groups); T_H1, R-squared=0.1533, p=0.0647 for low producers, R-squared=0.006748, p=0.2430 for high producers, p=0.3013 for the interaction term (slope*bacterial groups); T_{reg}, R-squared=0.0539, p=0.2538 for low producers; R-squared=0.1575, p=0.0925 for high producers, p=0.9930 for the interaction term (slope*bacterial groups)).

i, T_H17 cell percentages do not affect *C. rodentium*-encoded *espB* levels. *Citrobacter* colonization was measured by qPCR analyses detecting *espB* and plotted against T_H17 cell percentages in mice used for bacterial colonization experiments shown in Fig. 4g, Extended Data Fig. 5g, h were determined by qPCR and plotted against percentage of Th17 cells in individual mice. n=31, R squared=0.02928 for goodness of fit, F=0.9352, p=0.3414 for slope by simple linear regression. Dotted lines are 95% confidence bands of the best fit line.

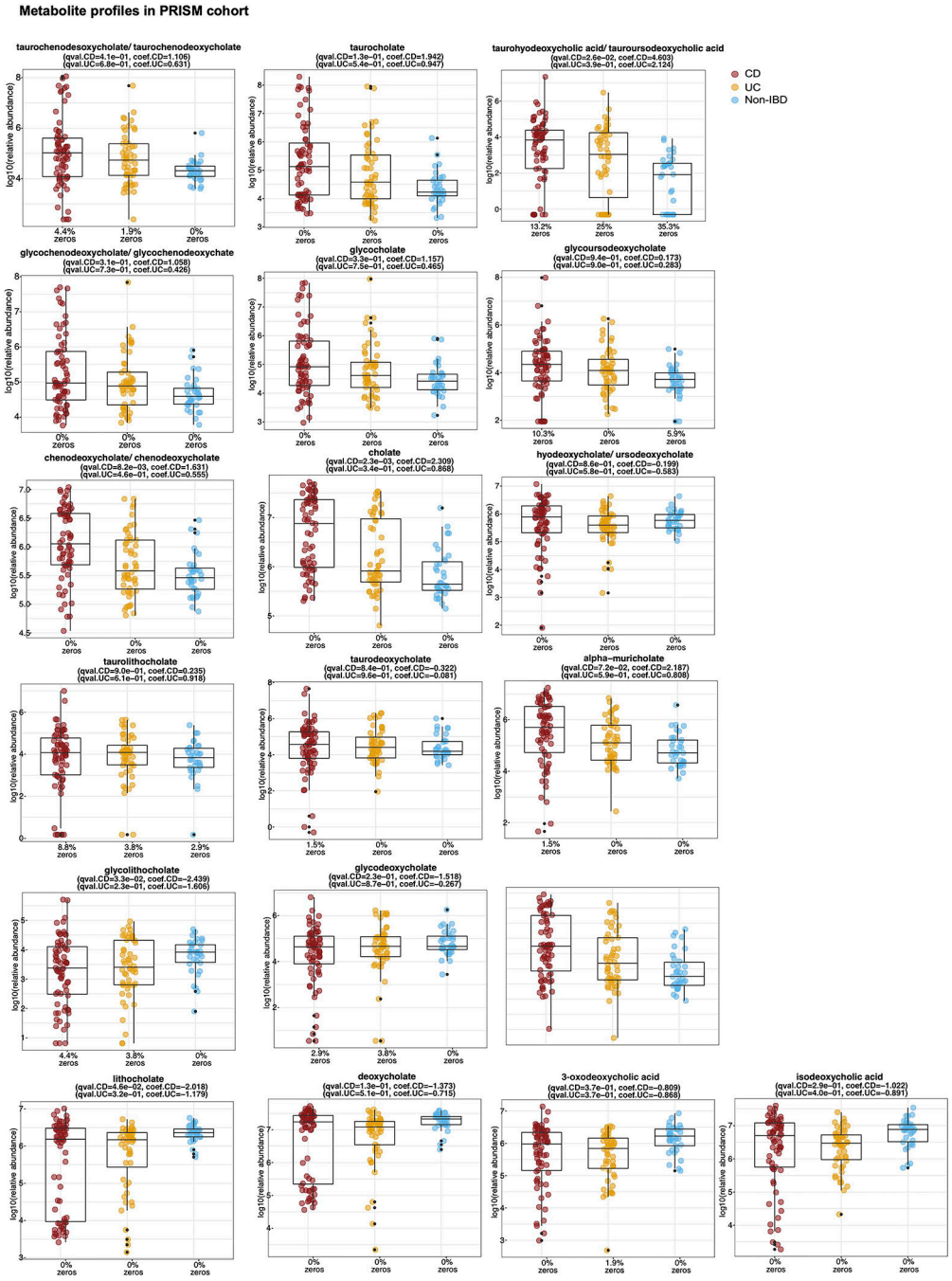

Extended Data Fig. 6 |. Levels of BA metabolites detected in the PRISM cohort.

Abundances of identifiable BAs in PRISM cohort. BA levels were not universally decreased in CD patients, indicating that decreased levels of LCA, 3-oxoLCA, and isoLCA were not due to lower levels of all BAs in these cohorts. Boxplots show median and lower/upper quartiles with outliers outside of boxplot ‘whiskers’ (indicating the inner fences of the data). n = 34 for CD, n=52 for UC and n=34 for non-IBD. The percentage of zeros in each condition are added as x-axis tick labels. See Table S6 for full results.

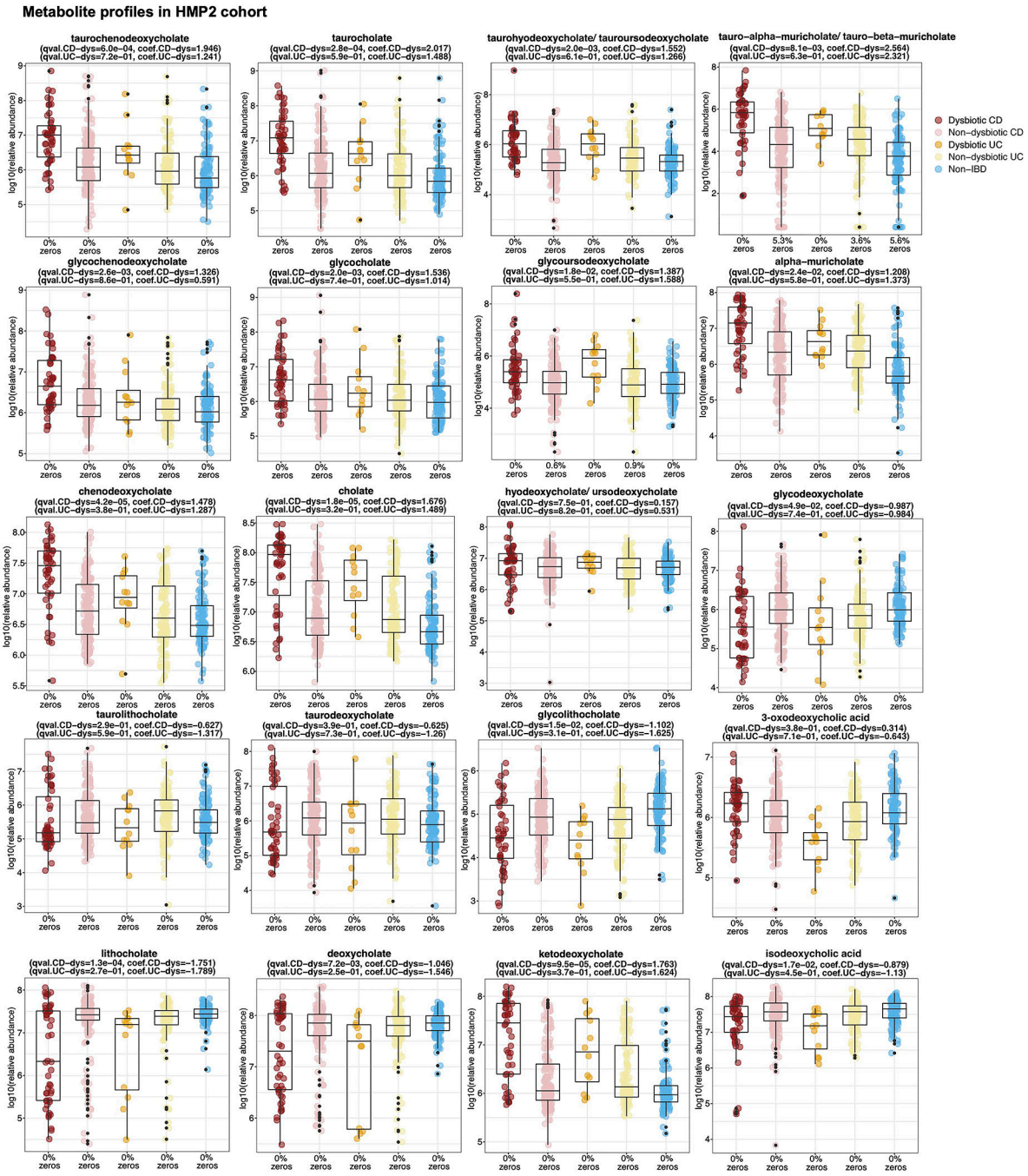

Extended Data Fig. 7 |. Levels of BA metabolites detected in the HMP2 cohort.

Abundances of identifiable BAs in HMP2 cohort. BA levels were not universally decreased in dysbiotic CD patients, indicating that decreased levels of LCA, 3-oxoLCA, and isoLCA were not due to lower levels of all BAs in these cohorts. Boxplots show median and lower/upper quartiles with outliers outside of boxplot 'whiskers' (indicating the inner fences of the data). n=47 for dysbiotic CD, n = 169 for non-dysbiotic CD, n=12 for dysbiotic UC, n=110 for non-dysbiotic UC and n=122 for non-IBD. The percentage of zeros in each condition are added as x-axis tick labels. See Table S6 for full results.

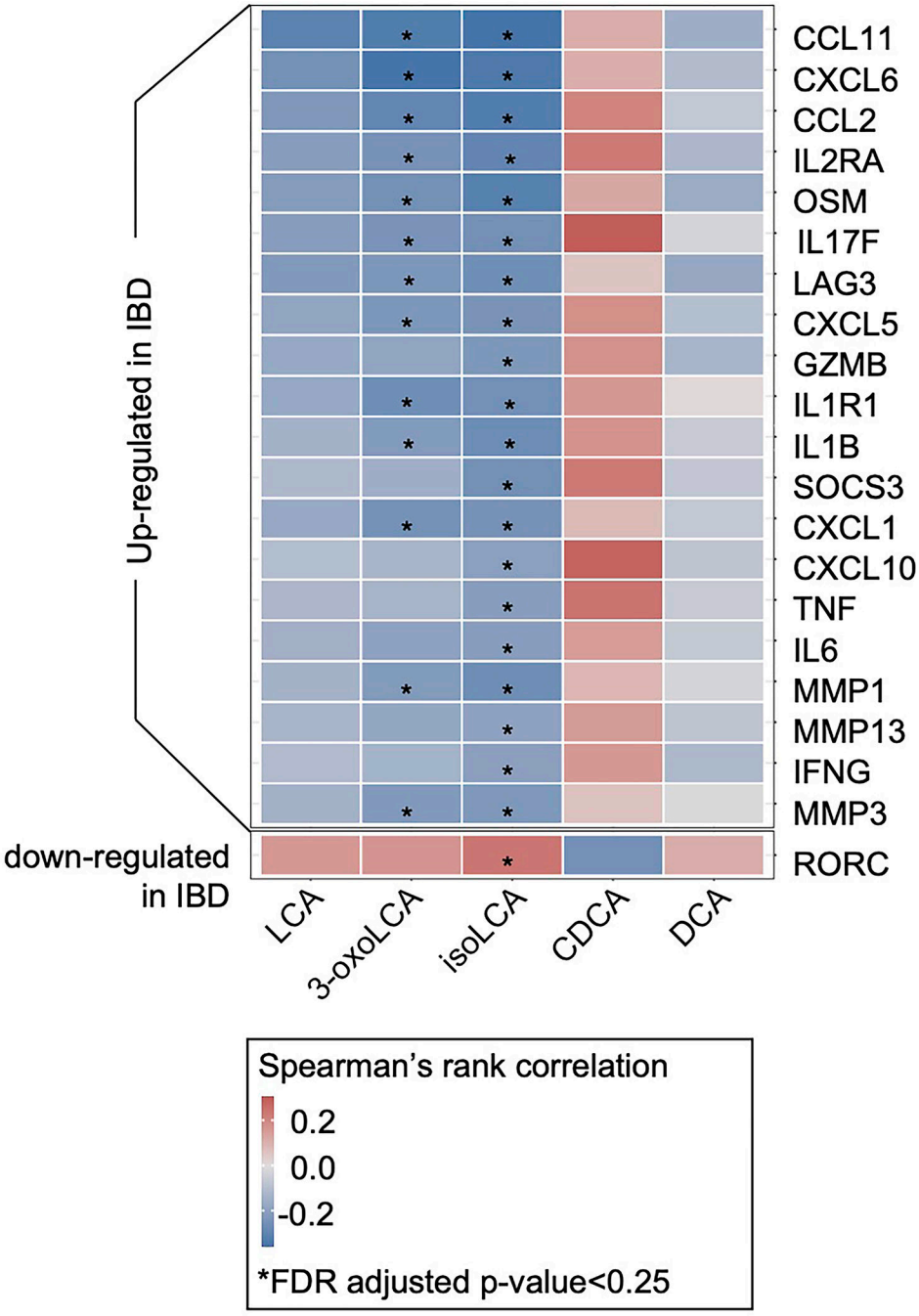

Extended Data Fig. 8 |. Correlation between T_H17/IL-17-related features and LCA metabolite abundance in HMP2.

T_H17/IL-17-related genes in IBD upregulated in IBD were significantly negatively correlated with 3-oxoLCA and isoLCA (FDR-adjusted *p*-value < 0.25) but not the other 3 control BAs (LCA, DCA, and CDCA). Differentially expressed T_H17/IL-17-related genes with at least one significant association are shown. This analysis was based on a subset of n = 71 subject-unique samples with matched metagenomic, metabolomic, and host transcriptomic profiling in the HMP2 cohort (33 CD, 21 UC, and 17 non-IBD controls, Spearman correlation with FDR adjusted *p*-value < 0.25). Correlations were based on

residual transcript and metabolite abundance after correcting for diagnosis, consent age, and antibiotic use. See Table S8 for full results.

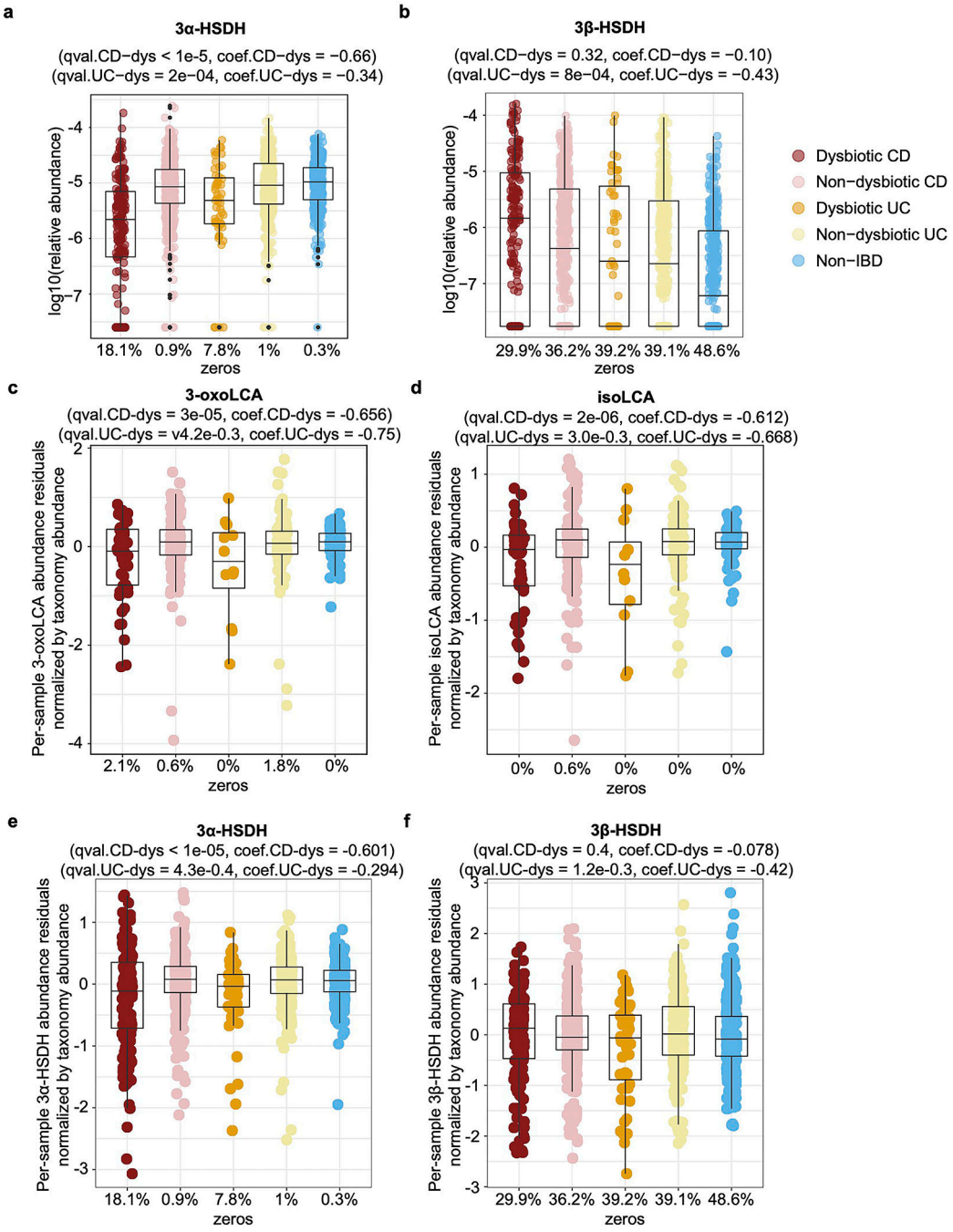

Extended Data Fig. 9 |. Correlation between 3α,β-HSDH-related microbial features and LCA metabolite abundance in HMP2.

a-b, Relative abundance distributions of differentially abundant 3α-HSDH (**a**) and 3α-HSDH (**b**) homologs profiled from HMP2 metagenomes (n = 1,595 samples from 130 subjects: linear mixed-effects model coefficient for dysbiosis within diagnosis, FDR-adjusted p-values < 0.05). Boxplots show median and lower/upper quartiles with outliers

outside of boxplot ‘whiskers’ (indicating the inner fences of the data). The percentage of zeros in each condition are added as x-axis tick labels. See Table S9 for full results. **c-f**, LCA metabolites show significant differential abundance after adjusting for variation in underlying taxonomic abundance. Accounting for underlying variation in the taxonomic abundance of the major producers of isoLCA (Actinobacteria and Firmicutes), we used the phyla abundances as additional covariates to normalize the abundance of LCA metabolites and enzymes. 3-oxoLCA (**c**) and isoLCA (**d**) as derived from metabolomic profiles of HMP2 cohorts are significantly depleted in HMP2 dysbiotic CD samples (n = 48) relative to non-dysbiotic controls (n = 169). Meanwhile, 3α-HSDH (**e**) and 3β-HSDH (**f**) homologs were also profiled from HMP2 metagenomes (n = 1,595 samples from 130 subjects; linear mixed-effects model coefficient for dysbiosis within diagnosis, FDR-adjusted p-values < 0.05). The percentage of zeros in each condition are added as x-axis tick labels. Boxplot ‘boxes’ indicate the first, second (median), and third quartiles of the data. The points outside of boxplot whiskers are outliers. Statistical analysis was performed using a linear mixed-effect model and its coefficient and significance, FDR-adjusted p-values, are shown.

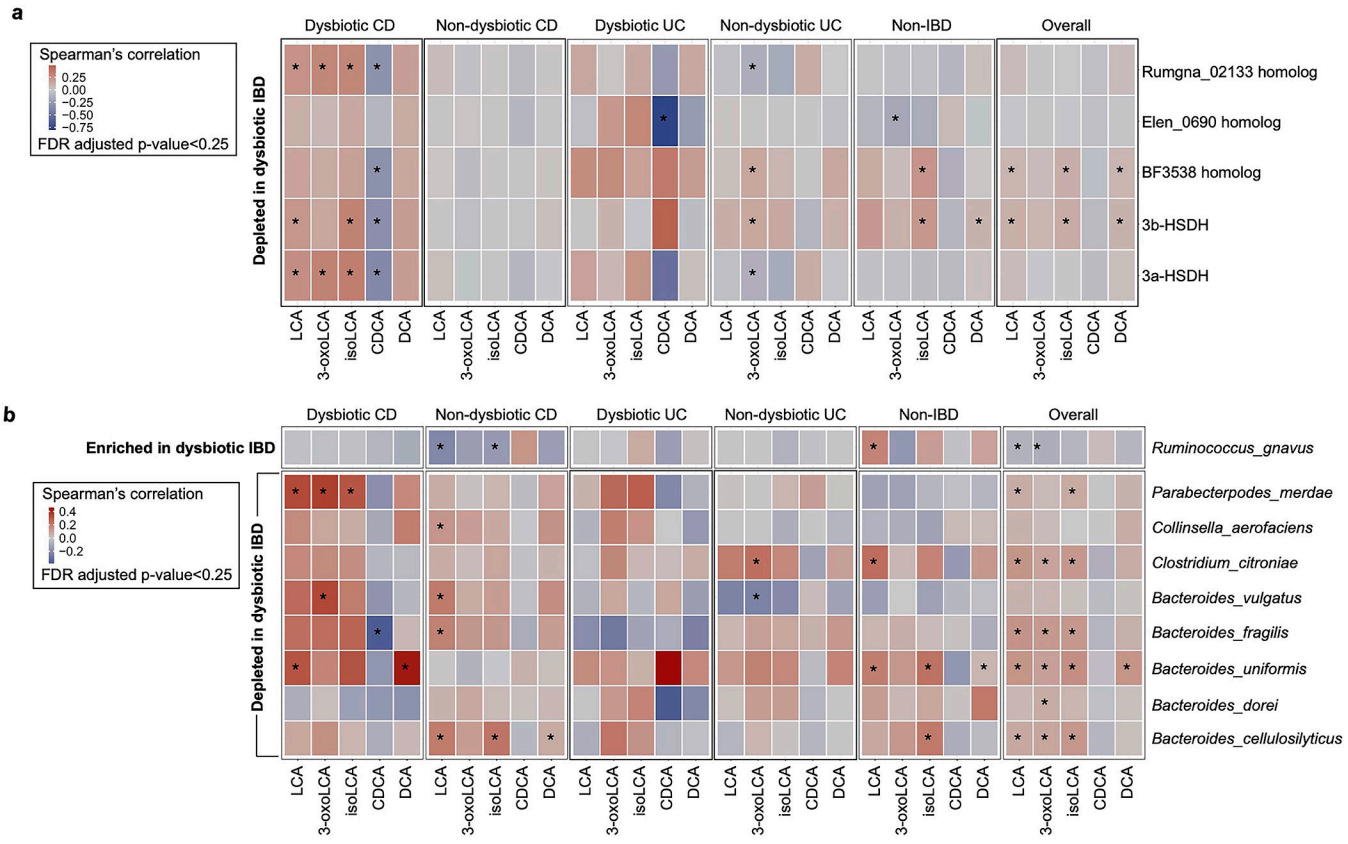

Extended Data Fig. 10|. 3α- and 3β-HSDH homologs and species with 3α-/ 3β-HSDH activity are likely to be positively correlated with 3-oxoLCA/ isoLCA in HMP2.

a, Differentially abundant 3α-/ 3β-HSDH homologs (FDR adjusted p-value < 0.05) with at least one significant metabolite association (Spearman correlation with FDR adjusted p-value < 0.25). Correlations were computed over a subset of paired metabolomes and metagenomes from the HMP2 cohort derived from 106 participants (CD, n=50; UC,

n=30; Non-IBD, n=26). **b,** Differentially abundant species with validated 3α-/ 3β-HSDH activity (FDR adjusted p-value < 0.05) with at least one significant metabolite association (Spearman correlation with FDR adjusted p-value < 0.25) with five metabolites are shown for the paired metabolome and metagenome samples from 106 participants (CD, n=50; UC, n=30; Non-IBD, n=26) in HMP2.

Supplementary Material

Refer to Web version on PubMed Central for supplementary material.

Acknowledgments

We thank members of the Devlin, Huh, and Clardy labs (Harvard Medical School-HMS) for helpful discussions. We thank the HMS ICCB-Longwood Screening Facility, BPF Genomics Core Facility at Harvard Medical School for their expertise and instrument support, N. Lee, J. Vasquez, C. Powell, Baylee Russell, and M. Henke for technical support and advice, and M. Trombly and S. Blacklow for critical reading of the manuscript. We thank Laurie E. Comstock for the pLGB30 plasmid (Addgene plasmid #126620) and Leonor García-Bayona for her technical support. We are grateful to the human patients who participated in the human stool screen, PRISM and HMP2 studies. We acknowledge NIH grant P30DK034854 and the use of the Harvard Digestive Disease Center's (HDDC's) core services, resources, technology and expertise. This work was supported by National Institutes of Health grants R01 DK110559 (J.R.H. and A.S.D.), R01AR074500 (P.J.T.), U54DE023798 (C.H.), R24DK110499 (C.H.), T32GM095450, and MIRA R35 GM128618 (A.S.D.), a Harvard Medical School Dean's Innovation Grant in the Basic and Social Sciences (A.S.D. and J.R.H.), a John and Virginia Kaneb Fellowship (A.S.D.), a Harvard Medical School Christopher Walsh Fellowship (L.Y.) and a Wellington Postdoctoral Fellowship (L.Y.). J.E.B was the recipient of a Natural Sciences and Engineering Research Council of Canada Postdoctoral Fellowship and is supported by the National Institute of Allergy and Infectious Diseases (K99AI147165). P.J.T. is a Chan Zuckerberg Biohub investigator. The computations in this paper were run in part on the FASRC Cannon cluster supported by the FAS Division of Science Research Computing Group at Harvard University. Figure panels in Fig. 2c, 4a, 4d, Extended Data Fig. 1b, c, Extended Data Fig. 3i, l were created using BioRender.

References

1. Hang S et al. Bile acid metabolites control TH17 and Treg cell differentiation. Nature 576, 143–148 (2019). [PubMed: 31776512]
2. Fiorucci S & Distrutti E Bile acid-activated receptors, intestinal microbiota, and the treatment of metabolic disorders. Trends Mol Med 21, 702–714 (2015). [PubMed: 26481828]
3. Ridlon JM, Kang D-J & Hylemon PB Bile salt biotransformations by human intestinal bacteria. J Lipid Res 47, 241–259 (2005). [PubMed: 16299351]
4. Modica S, Gadaleta RM & Moschetta A Deciphering the nuclear bile acid receptor FXR paradigm. Nucl Recept Signal 8, e005 (2010). [PubMed: 21383957]
5. Schaap FG, Trauner M & Jansen PLM Bile acid receptors as targets for drug development. Nat Rev Gastroentero 11, 55–67 (2014).
6. Guo C et al. Bile acids control inflammation and metabolic disorder through Inhibition of NLRP3 inflammasome. Immunity 45, 944 (2016). [PubMed: 27760343]
7. Ma C et al. Gut microbiome–mediated bile acid metabolism regulates liver cancer via NKT cells. Science 360, eaan5931 (2018). [PubMed: 29798856]
8. Cao W et al. The Xenobiotic transporter Mdr1 enforces T cell homeostasis in the presence of intestinal bile acids. Immunity 47, 1182–1196.e10 (2017). [PubMed: 29262351]
9. Duerr RH et al. A Genome-wide association study identifies *IL23R* as an inflammatory bowel disease gene. Science 314, 1461–1463 (2006). [PubMed: 17068223]
10. Nair RP et al. Genome-wide scan reveals association of psoriasis with IL-23 and NF-κB pathways. Nat Genet 41, 199–204 (2009). [PubMed: 19169254]
11. Consortium B et al. Genome-wide association study meta-analysis identifies seven new rheumatoid arthritis risk loci. Nat Genet 42, 508–514 (2010). [PubMed: 20453842]

12. Sakaguchi S Naturally arising CD4+ regulatory T cells for immunologic self-tolerance and negative control of immune responses. Annu Rev Immunol 22, 531–562 (2004). [PubMed: 15032588]
13. Josefowicz SZ, Lu L-F & Rudensky AY Regulatory T cells: mechanisms of differentiation and function. Immunology 30, 531–564 (2012).
14. Song X et al. Microbial bile acid metabolites modulate gut RORγ+ regulatory T cell homeostasis. Nature 577, 410–415 (2020). [PubMed: 31875848]
15. Campbell C et al. Bacterial metabolism of bile acids promotes generation of peripheral regulatory T cells. Nature 581, 475–479 (2020). [PubMed: 32461639]
16. Ivanov II et al. The orphan nuclear receptor RORγt directs the differentiation program of proinflammatory IL-17+ T helper cells. Cell 126, 1121–1133 (2006). [PubMed: 16990136]
17. Yang XO et al. T helper 17 lineage differentiation is programmed by orphan nuclear receptors RORα and RORγ. Immunity 28, 29–39 (2008). [PubMed: 18164222]
18. Hamilton JP et al. Human cecal bile acids: concentration and spectrum. Am J Physiol-gastr L 293, G256–G263 (2007).
19. Hirano S & Masuda N Transformation of bile acids by Eubacterium lentum. Appl Environ Microb 42, 912–915 (1981).
20. Devlin AS & Fischbach MA A biosynthetic pathway for a prominent class of microbiota-derived bile acids. Nat Chem Biol 11, 685–690 (2015). [PubMed: 26192599]
21. Ivanov II et al. Induction of intestinal TH17 Cells by segmented filamentous bacteria. Cell 139, 485–498 (2009). [PubMed: 19836068]
22. Esplugues E et al. Control of TH17 cells occurs in the small intestine. Nature 475, 514–518 (2011). [PubMed: 21765430]
23. Hong P-Y, Wu J-H & Liu W-T Relative abundance of Bacteroides spp. in stools and wastewaters as determined by hierarchical oligonucleotide primer extension. Appl Environ Microb 74, 2882–2893 (2008).
24. García-Bayona L & Comstock LE Streamlined genetic manipulation of diverse Bacteroides and Parabacteroides isolates from the human gut microbiota. mBio 10, e01762–19 (2019). [PubMed: 31409684]
25. Sayin SI et al. Gut microbiota regulates bile acid metabolism by reducing the levels of tauro-beta-muricholic acid, a naturally occurring FXR antagonist. Cell Metab 17, 225–235 (2013). [PubMed: 23395169]
26. Franzosa EA et al. Gut microbiome structure and metabolic activity in inflammatory bowel disease. Nat Microbiol 4, 293–305 (2019). [PubMed: 30531976]
27. Lloyd-Price J et al. Multi-omics of the gut microbial ecosystem in inflammatory bowel diseases. Nature 569, 655–662 (2019). [PubMed: 31142855]
28. Revu S et al. IL-23 and IL-1β drive human TH17 cell differentiation and metabolic reprogramming in absence of CD28 costimulation. Cell Reports 22, 2642–2653 (2018). [PubMed: 29514093]
29. Lee W et al. Multi-omics reveal microbial determinants impacting responses to biologic therapies in inflammatory bowel disease. Cell Host Microbe 29, 1294–1304 (2021). [PubMed: 34297922]
30. Sato Y, et al. Novel bile acid biosynthetic pathways are enriched in the microbiome of centenarians. Nature 599, 458–464 (2021). [PubMed: 34325466]
31. Bouladoux N, Harrison OJ & Belkaid Y The mouse model of infection with Citrobacter rodentium. Curr Protoc Immunol 119, 19.15.1–19.15.25 (2017). [PubMed: 29091261]
32. Huh JR & Littman DR Small molecule inhibitors of RORγt: targeting TH17 cells and other applications. Eur. J. Immunol. 42, 2232–2237 (2012). [PubMed: 22949321]
33. Patro R, Duggal G, Love MI, Irizarry RA & Kingsford C Salmon provides fast and bias-aware quantification of transcript expression. Nat Methods 14, 417–419 (2017). [PubMed: 28263959]
34. Love MI, Huber W & Anders S Moderated estimation of fold change and dispersion for RNA-seq data with DESeq2. Genome Biol 15, 550 (2014). [PubMed: 25516281]
35. Mi H et al. , Muruganujan A & Thomas P PANTHER in 2013: modeling the evolution of gene function, and other gene attributes, in the context of phylogenetic trees. Nucleic Acids Res 41, D377–D386 (2013) [PubMed: 23193289]

36. Browne HP et al. Culturing of “unculturable” human microbiota reveals novel taxa and extensive sporulation. Nature 533, 543–6 (2016). [PubMed: 27144353]
37. Hall AB et al. A novel *Ruminococcus gnavus* clade enriched in inflammatory bowel disease patients. Genome Med 9, 103 (2017). [PubMed: 29183332]
38. Yao L et al. A selective gut bacterial bile salt hydrolase alters host metabolism. Elife 7, e37182 (2018). [PubMed: 30014852]
39. Swann JR et al. Systemic gut microbial modulation of bile acid metabolism in host tissue compartments. Proc National Acad Sci 108, 4523–4530 (2011).
40. Chen I-MA et al. IMG/M v.5.0: an integrated data management and comparative analysis system for microbial genomes and microbiomes. Nucleic Acids Res 47, D666–D677 (2019). [PubMed: 30289528]
41. Mukherjee S et al. Genomes OnLine database (GOLD) v.7: updates and new features. Nucleic Acids Res 47, D649–D659 (2019). [PubMed: 30357420]
42. Drozdetskiy A, Cole C, Procter J & Barton GJ JPred4: a protein secondary structure prediction server. Nucleic Acids Res 43, W389–W394 (2015). [PubMed: 25883141]
43. Bisanz JE et al. A Genomic toolkit for the mechanistic dissection of intractable human gut bacteria. Cell Host Microbe 27, 1001–1013.e9 (2020). [PubMed: 32348781]
44. Segata N, Börnigen D, Morgan XC & Huttenhower C PhyloPhlAn is a new method for improved phylogenetic and taxonomic placement of microbes. Nat Commun 4, 2304 (2013). [PubMed: 23942190]
45. Yu G, Lam TT-Y, Zhu H & Guan Y Two methods for mapping and visualizing associated data on phylogeny using Ggtree. Mol Biol Evol 35, 3041–3043 (2018). [PubMed: 30351396]
46. Franzosa EA et al. Gut microbiome structure and metabolic activity in inflammatory bowel disease. Nat Microbiol 4, 293–305 (2019). [PubMed: 30531976]
47. Truong DT et al. MetaPhlAn2 for enhanced metagenomic taxonomic profiling. Nat Methods 12, 902–903 (2015). [PubMed: 26418763]
48. Suzek BE, Huang H, McGarvey P, Mazumder R & Wu CH UniRef: comprehensive and non-redundant UniProt reference clusters. Bioinformatics 23, 1282–1288 (2007). [PubMed: 17379688]
49. Franzosa EA et al. Species-level functional profiling of metagenomes and metatranscriptomes. Nat Methods 15, 962–968 (2018). [PubMed: 30377376]
50. Suzek BE et al. UniRef clusters: a comprehensive and scalable alternative for improving sequence similarity searches. Bioinformatics 31, 926–932 (2015). [PubMed: 25398609]
51. Mallick H et al. Multivariable association discovery in population-scale meta-omics studies. PLoS Computational Biology, 17(11): e1009442 (2021). [PubMed: 34784344]
52. Law CW, Chen Y, Shi W & Smyth GK voom: precision weights unlock linear model analysis tools for RNA-seq read counts. Genome Biol 15, R29 (2014). [PubMed: 24485249]
53. Smyth GK Bioinformatics and computational biology solutions using R and Bioconductor. Statistics Biology Heal 397–420 (2005) doi:10.1007/0-387-29362-0_23.
54. Barman M et al. Enteric salmonellosis disrupts the microbial ecology of the murine gastrointestinal tract. Infect. Immun. 76, 907–915 (2008). [PubMed: 18160481]
55. Sagaidak S, Taibi A, Wen B & Comelli EM Development of a real-time PCR assay for quantification of *Citrobacter rodentium*. J Microbiol Methods 126, 76–77 (2016). [PubMed: 27196638]

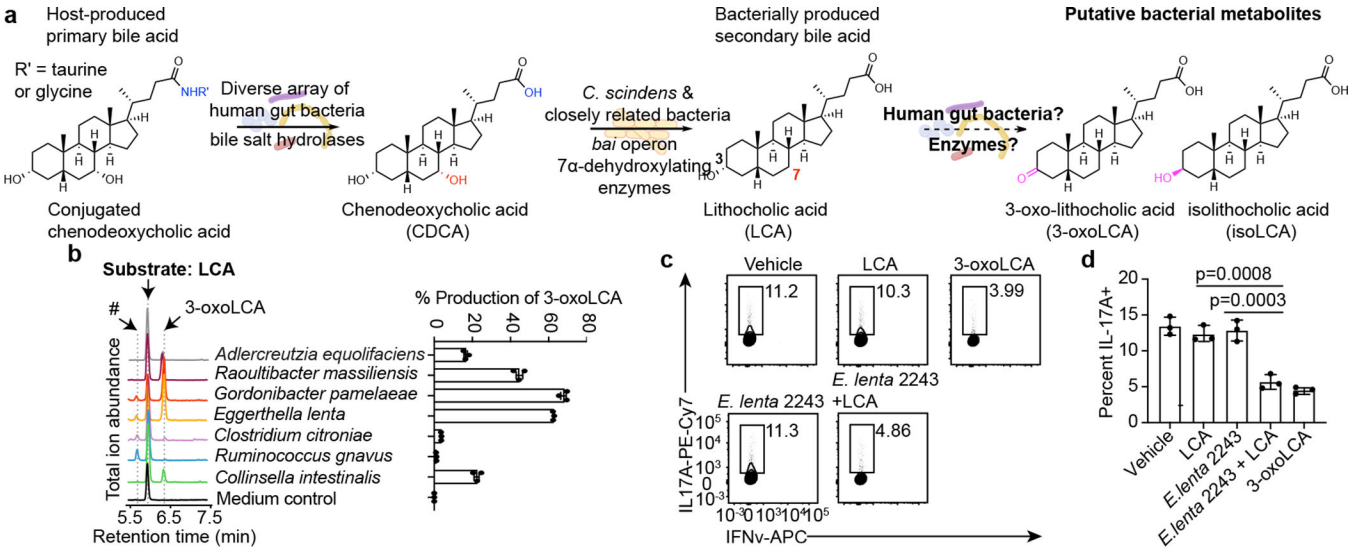

Fig. 1 |. Human gut bacteria produce 3-oxoLCA, a T_H17-modulating BA metabolite.

a, Bacterial conversion of host-produced BAs. Prior to this work, the bacterial strains and enzymes responsible for the conversion of lithocholic acid (LCA) to 3-oxolithocholic acid (3-oxoLCA) and isolithocholic acid (isoLCA) were not known.

b, Representative UPLC-MS traces (left) and percent production of 3-oxoLCA (right) by human bacterial isolates. Total ion chromatograms (TICs) are shown. An unknown peak of m/z 375.2 (#, retention time 5.7 min), was later identified as isolithocholic acid (isoLCA) (see Extended Data Fig. 2c) (n = 3 biological replicates per group, data are mean ± SEM). See Table S2 for full results.

c, d, Supernatants from *E. lenta* DSM2243 cultured with LCA inhibited T_H17 cell differentiation in vitro. Representative FACS plots (**c**) and population frequencies of mouse T_H17 cells (**d**) activated and expanded in vitro are shown. Naive CD4+ T cells from wild-type B6Jax mice were cultured under T_H17 cell polarizing conditions for 3 days and bacterial supernatants were added 18 hours after T cell receptor (TCR) activation (n = 3 biologically independent samples per group, data are mean ± SEM, one-way ANOVA followed by Tukey's multiple comparison test).

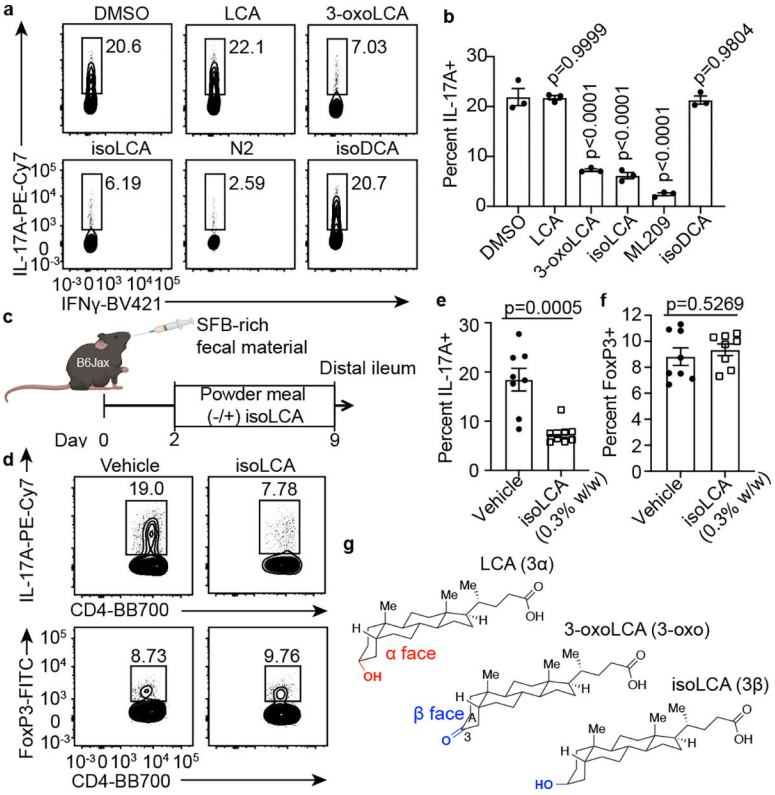

Fig. 2 |. The abundant gut bacterial metabolite isoLCA inhibits T_H17 cell differentiation.

a, b, IsoLCA inhibited the differentiation of mouse T_H17 cells in vitro. Representative FACS plots (**a**) and population frequencies of T_H17 cells (**b**) cultured in the presence of various BAs (20 μM) and ML209 (2 nM) (n = 3 biologically independent samples per condition, data are mean ± SEM, one-way ANOVA followed by Dunnett's multiple comparison test, vehicle set as control).

c-f, IsoLCA inhibited the differentiation of T_H17 cells in vivo. Experimental scheme (**c**), representative FACS plots (**d**) and population frequencies of T_H17 cells (**e**) and T_{reg} cells (**f**) in the ileal lamina propria of SFB-colonized mice are shown. B6 Jax mice were gavaged with SFB-rich fecal pellets and maintained on control or isoLCA-containing powder chow (0.3% w/w) for one week (n=8 mice per group, pooled from two experiments, data are mean ± SEM, two-tailed unpaired t-test).

g, Three-dimensional structures of 3-oxoLCA, isoLCA, and LCA showing the facial orientation of the C3 oxygenation.

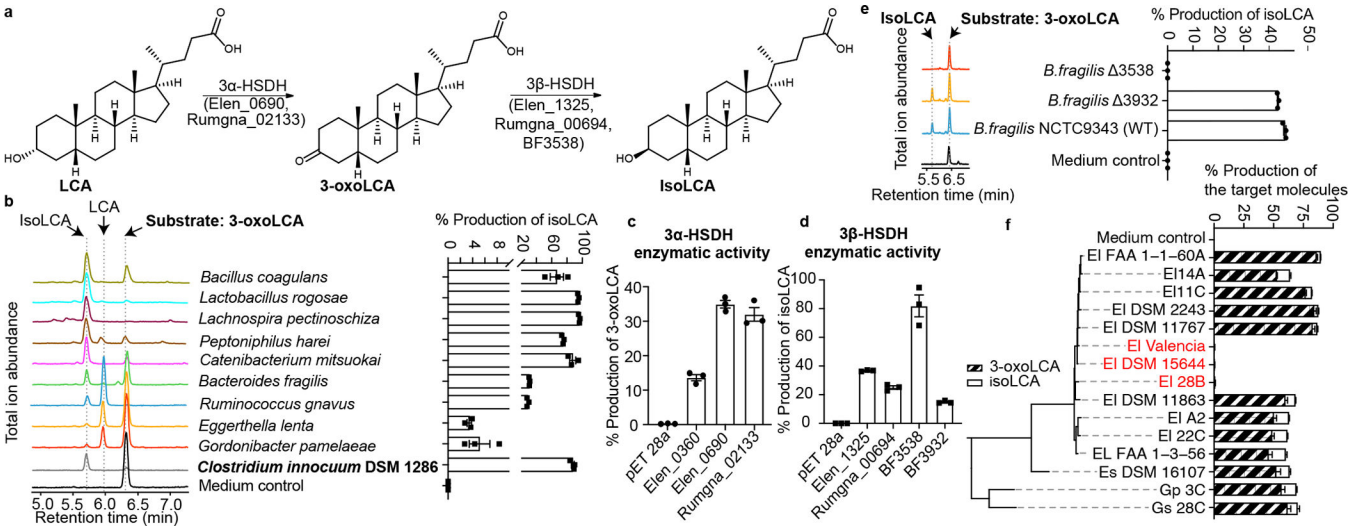

Fig. 3 |. Bacterial hydroxysteroid dehydrogenases (HSDHs) convert LCA to 3-oxoLCA and isoLCA.

a, Proposed biosynthetic pathway for the conversion of LCA to 3-oxoLCA and isoLCA.

b, Representative UPLC-MS traces (left) and percent production of isoLCA (right) by human bacterial isolates incubated with 3-oxoLCA (100 μM) for 48 hours. TICs are shown. *Clostridium innocuum,* which encoded 3β-HSDH homologs in HMP2 metagenomes (see Methods; Table S9), was selected for in vitro testing (n = 3 biological replicates per group, data are mean ± SEM, see Table S2).

c, d, Heterologous expression of candidate HSDHs from *E. lenta* DSM2243, *B. fragilis* NCTC9343, and *R. gnavus* ATCC29149 in *E. coli*. *E. coli* lysate was incubated with either 100 μM LCA (**c**) or 100 μM 3-oxoLCA (**d**) as a substrate. *E. coli* containing an empty vector was used as a control. Data are reported as percent conversion to product (either 3-oxoLCA or isoLCA) (n = 3 biological replicates per group, data are mean ± SEM, see Extended Data Fig. 4 and Figs. S1 and S10 for protein gels).

e, *B. fragilis* Δ3538, *B. fragilis* Δ3932, or the type strain *B. fragilis* NCTC9343 were incubated with 3-oxoLCA (100 μM) for 48 hours. Representative TIC UPLC-MS traces (left) and percent production of the target molecule isoLCA (right) are shown (n = 3 biological replicates per group, data are mean ± SEM, see Figs. S1 and S11 for DNA gels).

f, Cladogram of *E. lenta* and related human isolates and their production of 3-oxoLCA and isoLCA (El*, E. lenta*; Es, *Eggerthella sinensis*; Gs, *Gordonibacter sp.*, and Gp, *Gordonibacter pamelaeae*). *E. lenta* isolates in red (*E. lenta* 28B, *E. lenta* DSM15644, *E. lenta* Valencia) that lack a homolog of Elen_0690 did not synthesize 3-oxoLCA from LCA. All strains were incubated with 100 μM LCA for 48 hours (n = 3 biological replicates per group, data are mean ± SEM).

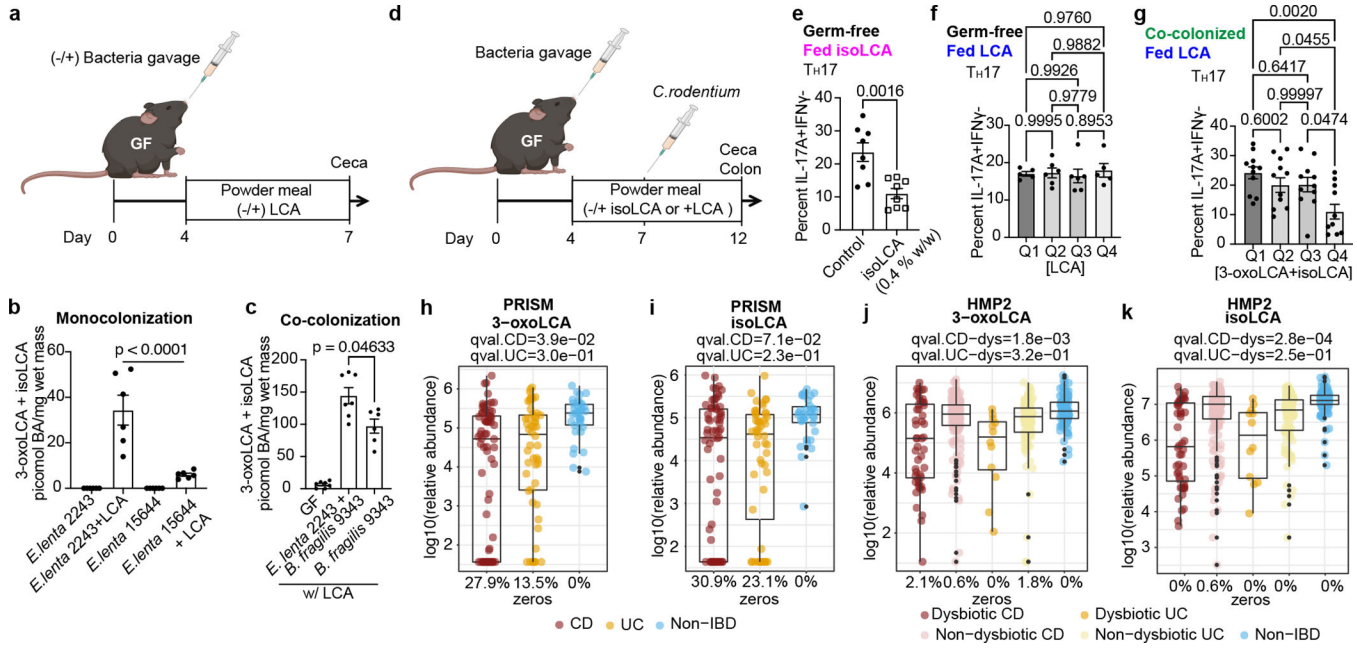

Fig. 4 |. 3-oxoLCA and isoLCA modulate T_H17 response in vivo and are negatively correlated with Crohn's disease in humans.

a, Experimental scheme for gnotobiotic experiments. Colonized mice were fed control chow or chow containing 0.3% LCA (w/w) and their cecal contents were analyzed by UPLC-MS for LCA metabolites.

b, **c**, GF-B6 mice were monocolonized with the *E. lenta* type strain (DSM2243) or a strain lacking a 3α-HSDH (DSM15644) (**b**) and were co-colonized with DSM2243 and *B. fragilis* NCTC9343 or monocolonized with *B. fragilis* (**c**). n=5, 6 for monocolonized and monocolonized+LCA groups, respectively (**b**); n=7, 7, 6 mice for GF, *E. lenta*+*B. fragilis*, and *B. fragilis* groups, respectively (**c**). IsoLCA was not detected in (**b**).

d, Experimental scheme for gnotobiotic experiments. GF mice were treated with a BA-containing diet in the presence or absence or prior colonization. Following *C.rodentium* infection, both IL-17A-producing CD4 T cell percentages in the colonic lamina propria and BA levels in the cecal contents of treated animals were analyzed.

e, IsoLCA feeding suppressed T_H17 differentiation in *Citrobacter*-infected GF mice (n=8 per group). Data are mean ± SEM pooled from two experiments, followed by two-tailed unpaired t test

f, LCA treatment did not significantly affect T_H17 cell levels in *Citrobacter*-infected GF mice treated with LCA-containing diets. Mice were sorted into quartile groups based on LCA levels in cecal contents (see Methods for details; Q1, lowest BA quartile, n=5 mice; Q2, n=6; Q3, n=6; Q4, highest BA quartile, n=5 mice).

g, Population frequencies of T_H17 cells were reduced in mice colonized with human gut bacteria producing higher compared to lower levels of 3-oxoLCA and isoLCA. Mice were sorted into quartile groups based on 3-oxoLCA+isoLCA levels in cecal contents (see Methods for details; Q1, lowest BA quartile, n=11 mice; Q2, n=12; Q3, n=11; Q4, highest BA quartile, n=11 mice). Data are mean ± SEM, followed by two-tailed unpaired t test (**e**) or

by one-way ANOVA by Dunnett's (**c**) or Tukey's multiple comparison tests (**b**, **f**, **g**); pooled from two (**b**, **c**), three (**e**, **f**), and six (**g**) experiments.

h-k, 3-oxoLCA and isoLCA were significantly depleted in CD subjects relative to controls in PRISM cohort (n = 34, 52, 34 for CD, UC, non-IBD) (**h**, **i**) and in dysbiotic CD samples relative to non-dysbiotic controls in HMP2 cohort (n=47,169, 12, 110, and 122 for dysbiotic CD, non-dysbiotic CD, dysbiotic UC, non-dysbiotic UC, and non-IBD, respectivley) (**j**, **k**). The percentage of zeros are added as x-axis tick labels. Boxplot 'boxes' indicate the first, second (median), and third quartiles of the data. Points outside of boxplot whiskers are outliers. Statistical analysis was performed using a linear mixed-model and its coefficient and significance, FDR-adjusted *p*-values, are shown (see Table S6).